The importance of inherent inorganics and the surface area of wood char for its gasification reactivity and catalytic activity towards toluene conversion

Agnieszka Korus[a,1] , Giulia Ravenni[b], Krzysztof Loska[c], Irena Korus[c], Abby Samson[d], Andrzej Szlęk[a]

[a] Department of Thermal Technology, Silesian University of Technology, Gliwice, Poland

[b] Department of Chemical and Biochemical Engineering, Technical University of Denmark, Lyngby, Denmark

[c] Department of Water and Wastewater Engineering, Silesian University of Technology, Gliwice, Poland

[d] Department of Mechanical Engineering, University of Sheffield, Sheffield, UK

Abstract

Gasification char is an effective catalyst for tar reforming because of the abundance of surface active sites, which are available for heterogeneous conversion of hydrocarbons and interactions with the reforming agents. This paper focuses on the importance of certain char properties for the gasification and catalytic reforming. Specifically, the gasification reactivity of spruce char is examined, along with its performance as a catalyst for toluene conversion. The material used for this work was produced via gasification of spruce wood chips in the pilot TwoStage Viking plant (Technical University of Denmark, Risø). To obtain a set of samples with varied surface

[1] Corresponding author, E-mail: agnieszka.korus@polsl.pl (Agnieszka Korus)

area characteristics and inorganic content, three pre-treatments were applied to samples of this char: acid washing, steam activation, and high-temperature treatment. The gasification and catalytic experiments performed with the untreated and modified materials revealed that the reactivity of the char during gasification in CO_2 depends mostly on the metal content in the sample, whereas the conversion of toluene was insensitive to the char inorganic content, but strongly correlated with the surface area available for heterogeneous reactions with toluene.

Keywords:

Char; gasification; inorganics; catalysis

1. Introduction

Biomass-derived char is the solid product of thermal conversion processes, such as pyrolysis and gasification. In the past, it has been often disposed as a waste; yet, nowadays, it is considered as an attractive material with versatile applications [1]. It is a heterogenous, carbon-rich substance, which generally has a porous structure and contains dispersed inorganics, such as Ca, K and Mg, that may have been present in the parent feedstock. Because of its properties and non-fossil origin, char represents a sustainable alternative to traditional materials and resources employed in applications ranging from agriculture, environmental management [2] and soil remediation [3], to energy storage [4] and catalysis [5].

Some types of char are particularly promising catalysts for hydrocarbon conversion, including reforming of the gasification tar for clean syngas production with a high H_2 content. Depending on the feedstock and the applied conditions, a diverse range of properties can be obtained; thus, the catalytic performance of the char in terms of tar conversion can vary from negligible to

45 nearly complete removal [6–9]. Several char properties are known to affect their catalytic
46 performance, including surface area, pore size distribution, O-containing surface
47 functionalities, and alkali and alkaline earth metal (AAEM) content, among others [8,10,11].

48 However, interactions between volatile hydrocarbons and the char matrix are complex, and the
49 exact mechanism and the role of various active sites are still debated. For example, while the
50 catalytic effect of AAEM species on char gasification is well-documented [12,13], conflicting
51 conclusions were drawn regarding their role in the conversion of various hydrocarbons, such as
52 methane [14–16].

53 Biomass-derived chars have a disordered, microcrystalline structure, which accommodates a
54 substantial number of active sites in the form of unsaturated carbon atoms with unpaired
55 electrons located at the crystallite edges and lattice defects [11,15,17]. Active sites catalyse
56 reactions at the char surface; during char activation with CO_2 or H_2O, these sites can also be
57 precursors for the formation of O-containing functional groups, such as carbonyl, carboxyl, and
58 quinone moieties. Such O-containing functionalities can be formed under inert atmosphere as
59 well, following the decomposition of certain polymeric constituents of biomass [10,14,18].

60 Metals incorporated in the carbonaceous lattice can also act as active sites. For example, C–O–
61 M or M_2O–C structures change the electron density at the neighbouring C atoms, thereby
62 enhancing the dissociative chemisorption of O from oxidising agents, such as H_2O or CO_2 [19–
63 22]. The O adsorption on the surface of the carbon lattice weakens the C–C bonds, allowing for
64 CO release from the char surface, which is the principle of char gasification. For this reason,
65 AAEM species are widely-recognised catalysts for the oxidation and gasification of
66 carbonaceous materials. However, the role that AAEM species play in the catalytic hydrocarbon
67 conversion process has not yet been entirely elucidated.

Several studies have reported enhanced tar decomposition due to AAEM species [18,23,24]. However, these studies were carried out in the presence of gasifying agents, such as CO_2 or H_2O. Therefore, the distinct role of the metals in the heterogeneous tar conversion process was unclear because of the concurrent effect of increased gasification and activation of the catalyst by these elements.

Fuentes-Cano et al. [25] studied naphthalene conversion using char under inert atmosphere, and observed a diminished catalytic activity for the acid-washed char. However, it is important to note that the char used in their study was derived from coal, which has a dispersion of metals that is different from that found in biomass [26]. Additionally, the char was acid-washed prior to the steam activation, so the latter process was also influenced by the removal of inorganics. Klinghoffer et al. [9] investigated the decomposition of methane over char and highlighted the importance of inorganics (Ca, Na, K, Mg, P, Si, and Fe) dispersed on the carbonaceous surface for catalysing the reactions. Similarly, Hervy et al. [27] studied the conversion of ethylbenzene and reported the importance of Ca, P, Al, and K oxides for the catalytic performance. In contrast, Dufour et al. [15] reported that the removal of inorganics from the pine char did not affect its methane reforming efficiency, and their observation was in agreement with some previous reports on the lack of catalytic activity of metals [16,17,28].

Recently, Feng et al. [24] reported a decrease in tar formation during gasification of K-loaded and Ca-loaded biomass at temperatures up to 700 °C. However, at all examined temperatures (500 – 900 °C), the relative yield of single-ring aromatics, especially toluene, increased significantly when AAEM-rich feedstock was used. Furthermore, in their studies regarding tar decomposition over activated biochar, Feng et al. [29] observed that the coke formation, which occurred primarily at AAEM sites, originated mainly from oxygenated hydrocarbons. These results suggest that O-containing hydrocarbons are more susceptible to the catalytic effects of AAEM species, whereas the decomposition of other tar components, such as light aromatics

with no heteroatoms, may be insensitive to the presence of these elements, and thus require independent investigations.

In this work, toluene was chosen as a representative of this class of compounds (i.e., light aromatics containing no heteroatoms). Studies involving this molecule are particularly relevant because toluene is among the most refractory and difficult tar species to remove from producer gas [7]. The objective of this work was to evaluate how the AAEM species inherently present in the char affect the heterogeneous conversion of toluene and the overall char gasification reactivity. The role and influence of inorganic species were also compared with the impacts of the surface area, porosity, and surface functional groups of each examined char.

Char derived from the gasification of spruce wood was selected for this study. With the goal of studying the effects of selected char properties, the obtained char was modified by dedicated pre-treatments (i.e., acid washing, steam activation, or high-temperature heat treatment), which can remove inorganics and modify the surface area and porosity of the char surface.

Prior to the toluene decomposition experiments, the gasification reactivity of chars was evaluated via thermogravimetric analysis in the presence of CO_2 as an oxidiser. The experiments involving toluene conversion and char gasification were conducted at 800 °C, which is above the minimum temperature where the catalytic effect of alkali metals is observed (approx. 700 °C) [19]. Toluene decomposition was carried out under an inert atmosphere to avoid the interference of the catalytic effect of inorganics on the char oxidation. Steam reforming tests were performed to verify the combined effects of AAEMs in the presence of both tar and a gasifying agent.

The novelty of this work lies in the parallel evaluation of the effects of selected char properties on gasification reactivity and catalytic performance of char for the decomposition of toluene. The results provide valuable insights into the relative importance of different key properties of

117 the char surface, which can be applied for the production of tailored carbonaceous catalytic
118 materials.

119

120 ## 2. Experimental (Materials and Methods)

121 ### 2.1. Materials

122 The char used in this study was generated from spruce wood chips using a pilot TwoStage
123 gasification plant (the Viking gasifier) operated at Technical University of Denmark (DTU)
124 Risø, in Roskilde, Denmark. Within the TwoStage process, biomass undergoes pyrolysis during
125 the first step, and it is then gasified in a separated reactor. In this second stage, an air inlet allows
126 for partial oxidation of the tar and locally increases the temperature up to 1100 °C. Additional
127 details about the TwoStage gasification process can be found in the literature [30,31]. The
128 Viking char (VC) used in this study was collected directly from the solid residues of the
129 gasification plant. The char from the Viking gasifier has a large surface area with well-
130 developed mesoporosity resulting from its participation in the reforming process. These
131 properties made it an efficient catalyst for the conversion of tar model compounds and real tar
132 mixtures [32,33]. The diversified catalyst properties investigated in this work were obtained by
133 applying pre-treatments to subsampled batches of the original char. The final VC has a stable
134 carbon structure because of the high temperatures reached during the TwoStage process.
135 Therefore, it can be assumed that the applied pre-treatments induced negligible variations in
136 the carbonaceous structure, i.e., the aromaticity or microcrystalline arrangement. These features
137 contribute significantly to the catalytic performance of chars, and they are closely related to the
138 type of feedstock and the conditions of char formation [11]. Thus, it is crucial that the
139 experimental modifications maximise the changes in the AAEM content and surface area while
140 maintaining a similar carbon structure in all studied samples. Prior to any treatment, VC was

ground in an agate mortar and sieved to isolate particles in the 250-600 μm size range, selected based on the reactor size and the reports on similar studies [8,32].

Three different pre-treatments were applied to three different subsamples of the raw material (VC), specifically, (i) acid (HCl) washing to remove inherent inorganics, (ii) steam activation to increase the surface area, and (iii) thermal treatment at 1000 °C under N_2 to reduce char porosity. In the first pre-treatment, aimed at the removal of inorganics, two cycles of acid wash were performed by shaking the subsample of VC in 2M HCl solution for 24 h. After the second cycle, the char was washed with distilled water to remove Cl^- ions (verified by addition of $AgNO_3$ to the filtrate). The char was then vacuum filtered and dried at 60 °C under N_2 flow until a constant mass was reached. This modified VC char was referred to as VC_HCl. To increase the surface area, another VC subsample was subjected to steam activation by heating a fixed bed of char up to 800 °C in a quartz tube reactor under N_2 flow, followed by 120 min of isotherm under a flow of 15/85 vol.% of H_2O/N_2. The char was then cooled to ambient temperature under N_2 flow and referred to as VC_SA. This pre-treatment also increased the AAEM concentration in the char due to the carbon burn-off. The last modification involved the heat treatment of the VC. A fixed bed of the third VC subsample was heated at a rate of 10 K/min up to 1000 °C, maintained at that isothermal condition for 180 min, and then cooled to ambient temperature, all under N_2 flow. The goal of this procedure was to modify the pore distribution of the sample by inducing pore collapse and/or sintering. The obtained material was referred to as VC_HT.

These pre-treatments produced a set of samples with similar carbonaceous structure yet varying surface areas and concentrations of inorganics, thus enabling investigations into the individualised effects of these two parameters on the activity of char.

2.2. Char analysis

Different techniques were applied to characterise the fresh chars and verify the outcomes of the pre-treatments. In addition, the spent chars recovered after 50 min of toluene conversion tests were analysed to determine the effect of the heterogeneous reaction on the char properties.

The C, H, N, and S (CHNS) contents were determined with an elemental analyser (EA3000, EuroVector, Italy) and assessed on a dry basis. Since negligible amounts of S and N were detected in the samples, only the H/C ratios are reported in this work. At least three repetitions of each measurement were carried out, and the averaged values with standard deviations are reported.

The Na, K, Ca, Mg, and Fe contents in the bulk of the char were analysed with a SpectrAA 880 Varian Atomic Absorption Spectrometer (AAS) after sample digestion with HNO_3 in a Milestone MLS1200 MEGA microwave. Because of the strong heterogeneity of the chars, four repetitions of each sample measurement were performed, and the averaged values with standard deviations are reported.

The surface functional groups on the chars were examined via attenuated total reflectance Fourier transform infrared (ATR-FTIR) spectroscopy using a Perkin Elmer Spectrum 100 spectrometer with a Universal Attenuated Total Reflectance module equipped with a germanium crystal. Each spectrum was constructed from 32 scans, with a resolution of 4 cm^{-1} within the range of 4000-700 cm^{-1} wavenumbers. The averaged spectra of five measurements are reported herein for each material.

The surface area and pore size distribution (PSD) of each sample were analysed with a Micromeritics TriStar II 3020 analyser. The samples were outgassed under N_2 flow at 200 °C for 24 h prior to the analysis; the adsorption-desorption isotherm of N_2 at 77 K was performed for the relative pressures (p/p_0) in the range of 0-0.95, and the CO_2 adsorption at 273 K was

carried out for p/p_0 up to 0.03. Two separate calculations regarding the surface area of each char were performed using the Brunauer-Emmett-Teller (BET) model, specifically, one from the N_2 adsorption isotherm that accounted for the mesopores and some of the micropores, and the other for the CO_2 adsorption data, which accommodated the whole micropore range. Additionally, for comparison, the surface area of the micropores was estimated using the t-plot method applied to the N_2 adsorption data and using a statistical thickness curve (Carbon Black STSA). All measurements were carried out in duplicate, and the averaged values with standard deviations are reported. The PSD was calculated using the two-dimensional version of non-local density functional theory (2D-NLDFT) [33] and the kernels for slit pore carbon that were included in the Micromeritics software. Combining data from N_2 and CO_2 adsorption allows for a more detailed PSD analysis of the materials wherein a significant fraction of pores are narrower than 7 Å [33].

The structure and chemistry of the char surface were also evaluated with a scanning electron microscope (Prisma E, Thermo Scientific) coupled to an energy dispersive spectroscopy detector (SEM-EDS). For each sample, several transversal and longitudinal sections were examined to account for the strongly heterogenous structure of the chars.

2.3. Reactivity and kinetic parameters calculation

Char reactivity during gasification with CO_2 was examined by thermogravimetric analysis (TGA) performed with a Netzsch STA 409 LUXX instrument, according to the following procedure: 5 mg of the sample was heated up to 1000 °C at a 10 K/min rate under 100 mL/min N_2 flow, and then cooled to the desired gasification temperature (800, 850, or 900 °C); after 15 min of N_2 purging, the flow was changed to 50/50 vol.% CO_2/N_2, and the char was gasified under isothermal conditions until a constant residual mass was reached. For all fresh and spent

chars, the gasification was carried out at 800 °C, and the registered mass loss was used to calculate the gasification reactivity. Additionally, for VC and VC_HCl, the tests at 850 and 900 °C were performed to determine the kinetic parameters of the gasification reaction. All tests were carried out in duplicate; the averaged values with corresponding standard deviations are reported for the char reactivities. For the kinetic parameters, to account for a kinetic compensation effect, raw data from both repetitions were averaged prior to calculating the activation energy and the pre-exponential coefficient.

The reactivity at 50 % conversion (R_{50}) can be determined using Eq. 1 [34],

$$R_{50} = k_0 \exp(-E/RT) p_{CO_2}^n \quad (1)$$

where k_0 is the pre-exponential factor ($bar^{-n} \cdot s^{-1}$), E is the activation energy ($kJ \cdot mol^{-1}$), R is the gas constant ($kJ \cdot mol^{-1} \cdot K^{-1}$), T is the absolute temperature (K), p_{CO_2} is the partial pressure of CO_2 (bar), and n is the reaction order. This analysis was applied to examine the influence of the pre-treatments on the gasification of the VC char.

The representative R_{50} value for the 20-80 % conversion of each sample was calculated using data obtained from the TGA tests of char gasification at 800 °C, according to the procedure described by Ollero et al. [34]. The conversion of the sample was determined from Eq. 2

$$X_i = (m_0 - m_i)/(m_i - m_a) \quad (2)$$

where m_0 is the initial mass of the sample, m_i is the mass at each time, and m_a is the mass of the ash that remained after the conversion.

The reactivity R_i at each time was calculated for each datapoint using Eq. 3

$$R_i = (-\mathrm{d}m_i/\mathrm{d}t)/(m_i - m_a) \quad (3)$$

The first estimate of normalised structural profile function for each datapoint was determined from Eq. 4

$$F_i = R_i / R_{50} \tag{4}$$

where R_{50} is the first estimate of the reactivity at 50 wt.% conversion. Then, the 5th order polynomial function was fitted to the $F_i - X_i$ data to obtain the normalised structural profile $F(X)$.

Finally, the weighted mean value of R_{50} was calculated using Eq. 5,

$$R_{50} = \frac{\sum_i \omega_i R_i / F(X)}{\sum_i \omega_i} \tag{5}$$

where ω_i is the statistical weight determined as $\omega_i = R_i(1 - X_i)$.

The kinetic parameters for VC and VC_HCl were calculated based on the reactivities measured at 800, 850, and 900 °C, under the assumption of an Arrhenius-type temperature dependence, using the linear equation presented in Eq. 6:

$$\ln R_{50} = \ln k_0 - \left(\frac{E}{RT}\right) + n \ln\left(p_{CO_2}\right) \tag{6}$$

Only one partial pressure of CO_2 was examined; thus, the reaction order, n, was assumed *a priori* to be 0.36, based on the data available in the literature [34].

To correlate the reactivity of the chars with their specific properties, the R_{50} values were used as a parameter to link the specific surface area of the samples with their inorganic content, represented by K, which is one of the most reactive AAEM.

2.4. Toluene conversion tests

The catalytic performances of the untreated and modified chars during the conversion of toluene were assessed by examining its conversion over a fixed bed of char in a laboratory quartz tube reactor. Specifically, the heterogenous conversion of toluene over the different chars was assessed in pyrolytic conditions (N_2 atmosphere) at 800 °C, for either 30 or 50 min. The VC and VC_HCl samples were also tested under oxidising conditions, with 15 vol.% of steam in N_2, during 50 min of steam reforming of toluene at 800 °C.

The test rig, described in detail in previous work [35], allowed for the pre-mixing of gaseous reactants in the evaporator. Toluene (and water if steam was required) were fed through a syringe pump into the individually-controlled heating section filled with quartz wool and purged with N_2. Vapours were then introduced into the main reactor containing the fixed char bed maintained at the desired reaction temperature. The condensable reaction products were captured downstream of the reactor in the cooled impinger bottles filled with dichloromethane, and analysed post-run with GC-FID; the permanent gases were analysed online with GC-TCD. The blank tests revealed that the efficiency of the sampling train was above 98 % and the toluene thermal decomposition in the absence of a catalytic bed was negligible. The procedures for the pyrolytic and reforming tests, detailed in previous work, were followed closely [35,36]; the only difference was that the gas analysis was performed online with a 10 min interval required to separate the released gases. Toluene was fed with a constant concentration of 12 g/Nm^3 for either 30 or 50 min. Two types of reaction were examined: pyrolytic conversion under pure N_2, and steam reforming under 15/85 vol.% H_2O/N_2 flow. Temperature, and toluene and steam concentrations that were applied for the conversion tests were based on the reports on similar studies [7,9,35,36] to enable the comparison with other catalytic materials. After each measurement, the char bed was cooled to ambient temperature under N_2 flow; the physicochemical properties of the spent materials were analysed along with the fresh chars to

evaluate the changes that occurred during the reactions with toluene (and steam for the reforming tests). All runs were carried out in duplicate, and the averaged values with standard deviations are reported. The results of the toluene conversion tests were used to calculate the toluene conversion, η_T, from Eq. 7,

$$\eta_T = \left(m_f - m_r\right)/m_f \cdot 100\% \quad (7)$$

where m_f and m_r represent the mass of toluene (mg) fed into the reactor and recovered in the impingers, respectively. The η_T values were then used to estimate the catalytic performance of each material and to determine the correlation between specific properties of the tested chars, as reported in Sections 3.3 and 3.4, respectively.

An overview of the char samples produced from pre-treatments of VC and the corresponding spent samples after toluene conversion is presented in Fig. 1. The pyrolytic conversion tests (N_2) allowed for evaluation of the direct roles of inorganics and surface area of char on the heterogenous reactions with toluene. The reforming tests (Steam) were aimed at the evaluation of the indirect role of inorganics, i.e. their catalytic effect on char oxidation that occurred concurrently, yet independently, to the toluene conversion, when steam was present. Thus, the reforming tests were limited to the original char (VC) and the sample with the removed inorganics (VC_HCl).

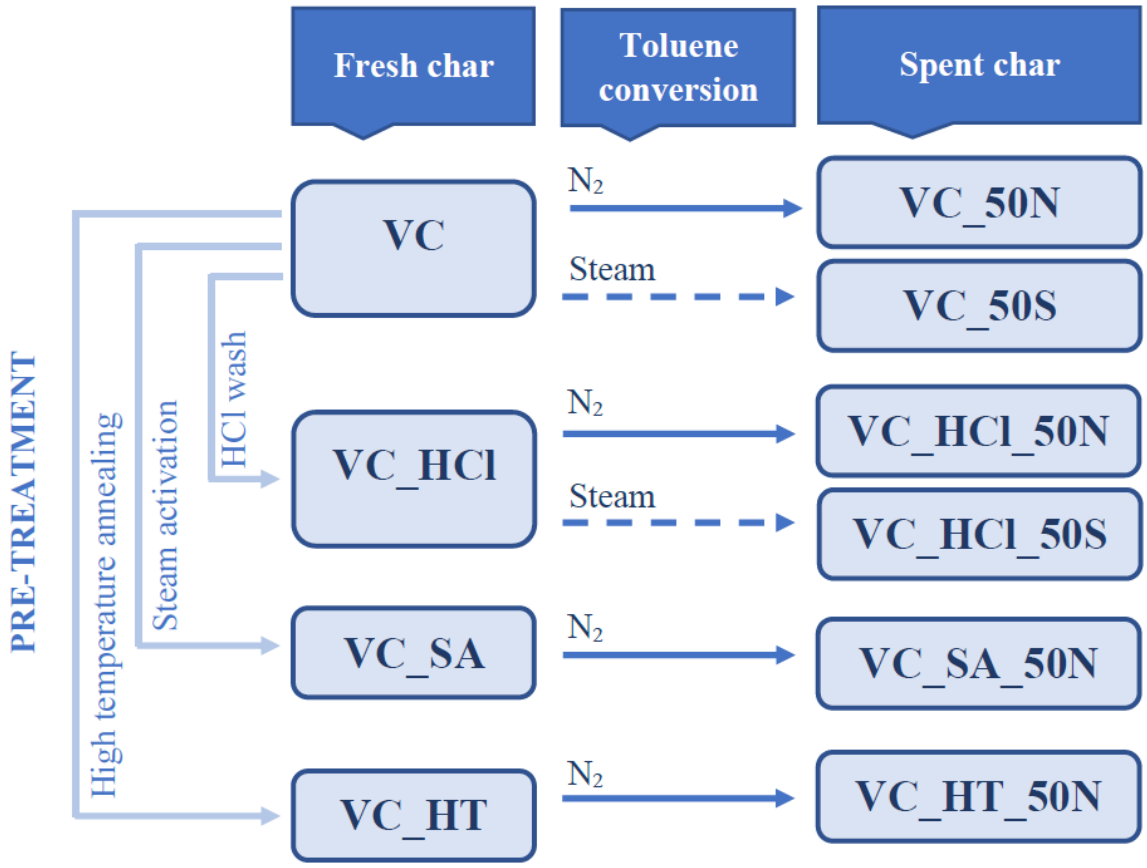

297

298 Fig. 1. Schematic describing the toluene decomposition experiments under nitrogen or steam
299 catalysed by untreated and modified VC.

300

301 **3. Results and discussion**

302 **3.1. Physicochemical properties of chars**

303 The applied pre-treatments provided a set of chars with various properties, and the fresh chars
304 were analysed to relate these properties to the observed gasification reactivity and activity
305 towards toluene removal. The spent chars were also examined to better understand the nature
306 of the heterogenous conversion of toluene.

The analysis of the CHNS content in the fresh and spent samples revealed either non-detectable or negligible amounts of N and S in all chars; the atomic H/C ratios are presented in Fig. 2. The untreated Viking char (VC) had the highest share of H atoms in the structure, and all applied pre-treatments resulted in a decrease of the relative amount of H. This was likely because of the dehydrogenation of the char under high temperatures (VC_HT), the formation of larger aromatic structures due to interactions with steam (VC_SA), and the removal of lighter H-rich labile compounds during the acid wash (VC_HCl).

The coke formed during tar conversion is usually low in H because of the dehydrogenation of aromatic tar compounds that occurs during their polymerisation on the catalyst surface. Thus, the chars recovered after toluene pyrolysis had lower H/C ratios, with the exception of VC_SA. As revealed by the comparison of VC and VC_SA, the steam activation drastically diminished H/C ratio of the char. Therefore, it is possible that the toluene-derived coke deposited on the spent char had higher H content than the fresh VC_SA, resulting in the increased H/C ratio in VC_SA_50N.

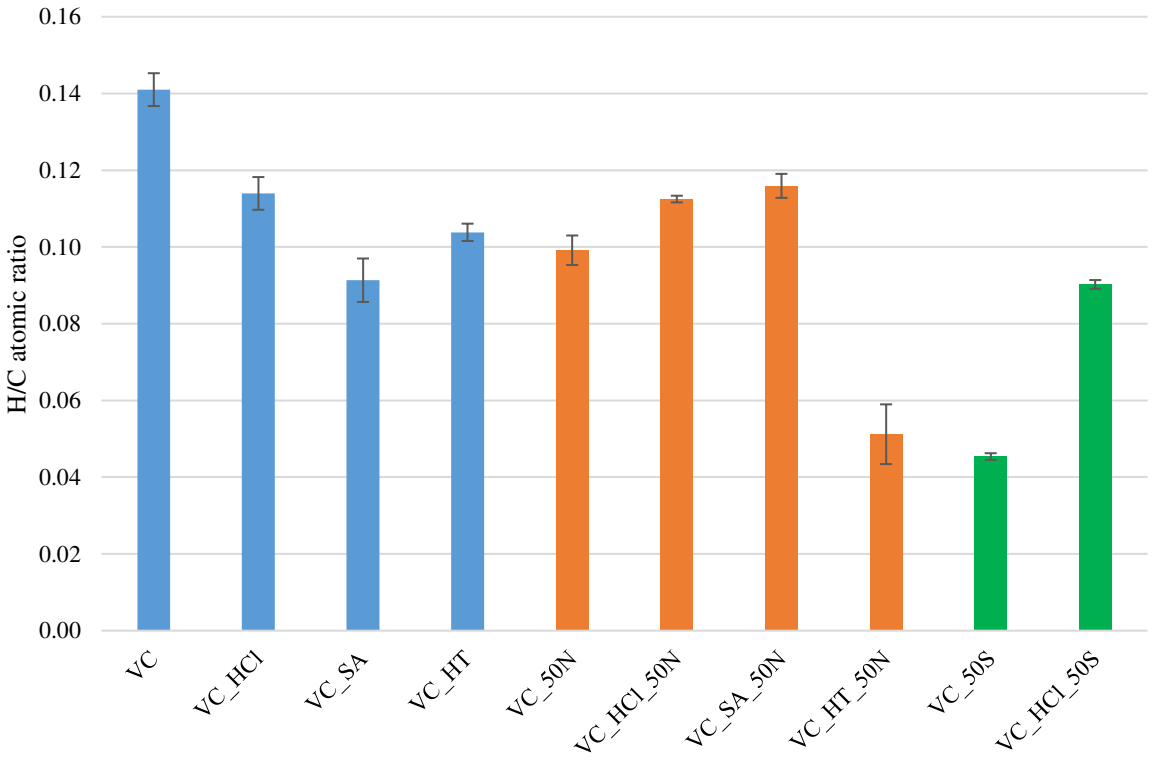

Fig. 2. The H/C atomic ratios in the untreated (VC) and modified (VC_HCl, VC_SA, VC_HT) Viking chars, both fresh and recovered after 50 min of toluene pyrolysis (50N) or steam reforming (50S)

3.1.1. Metal content in chars

The AAS results illustrating the content of the most common AAEMs and Fe in biochars are presented in Fig. 3. Despite the strong heterogeneity of the samples, which leads to high uncertainties in the measured values, some statistically significant differences were observed. The acid washing removed the AAEM species almost completely; K content was reduced by 99 wt.% and Ca by 98 wt.% in the VC_HCl sample. Fe was more resilient to the treatment; only 76 wt.% of this element was removed, making Fe the most abundant metal in the analysed VC_HCl. Steam activation of VC caused carbon burn-off, resulting in a 2-3 times higher concentration of metals in the VC_SA, compared with the untreated char. A slight reduction in the concentration of inorganics in the bulk of the char was observed after the high-temperature thermal treatment (VC_HT), likely due to partial vaporisation of the ash fraction.

Toluene conversion under an inert atmosphere led to intense coke formation, resulting in an increased carbon content in the spent catalyst. However, no significant decrease in the concentration of inorganics was observed, except in the case of the VC_SA char.

During toluene decomposition in the presence of steam, the steam reforming of carbon caused an increased concentration of metals in the VC_50S. The same effect was not observed in the VC_HCl_50S sample, which underwent less intense gasification reactions, as discussed further in Section 3.3.

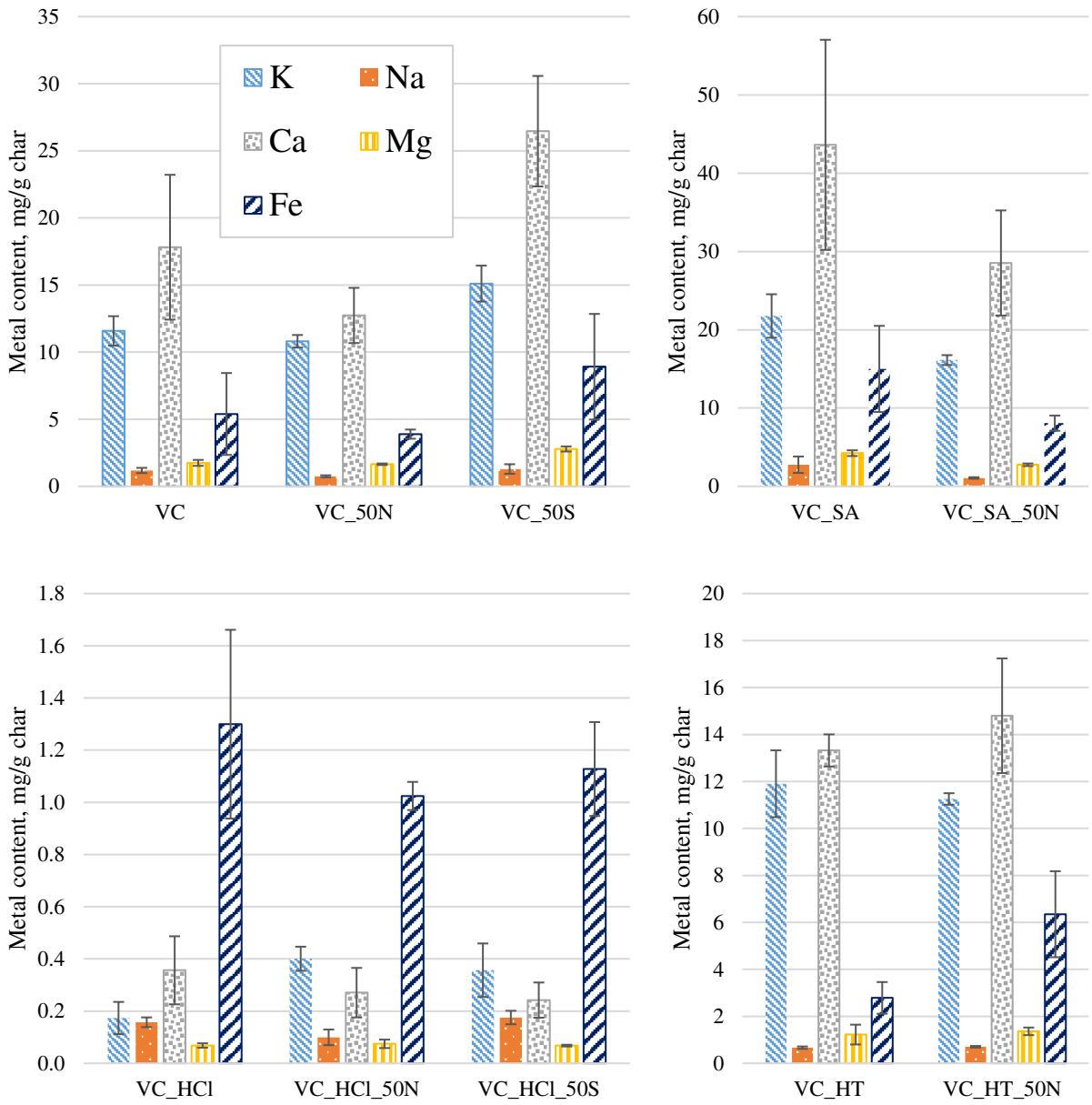

Fig. 3. Content of selected metals in the fresh Viking char (VC), acid-washed VC (VC_HCl), steam-activated VC (VC_SA), and high-temperature annealed VC (VC_HT), as well as in spent chars recovered after 50 min of toluene conversion under pure nitrogen (50N) or 15 vol.% of steam (50S)

3.1.2. SEM-EDS analysis

The dispersion of the reactive elements on the surface of each char was assessed using SEM-EDS. As shown in Fig. 4, the surfaces of all char samples were strongly heterogeneous, and the measured concentrations varied in different areas of the same material. Therefore, the mean concentration values for the analysed surfaces were used to evaluate the differences between the materials.

Unsurprisingly, C (not shown) and O were the most abundant elements detected on the surface of all samples. The C concentration on the surface of the char samples was in agreement with the values obtained from elemental analysis. In comparison with VC, the chars obtained following all applied pre-treatments and the spent chars all contained reduced amounts of O on their surface. The diminished oxygen presence in the EDS spectra is consistent with the destruction of some O-containing surface functionalities, as revealed by ATR-FTIR analysis.

The most abundant inorganic species detected on the surface of fresh char samples were Ca and K, followed by Fe and Mg, in good agreement with the AAS results. In addition, Si and traces of S, P, and Na were detected. The surface concentrations of some AAEM species, namely K, Ca, and Mg, were higher than the values measured with the AAS technique, which examined the bulk volume of the sample, suggesting that these elements accumulated on the char surface. The VC is a gasification residue, meaning it is the product of numerous volatile-solid interactions, which are known to induce the migration of AAEM species towards the char surface [10,37].

Compared with VC, higher concentrations of K and Ca were detected on the surface of VC_SA and VC_HT samples. Since the heat treatment did not significantly change the bulk concentration of these metals, the presence of these inorganic regions at the surface suggest that the applied thermal treatment may have caused the migration of metal atoms towards the surface

of the catalyst, as previously observed by Klinghoffer et al. [14]. The accumulation of metals on the surface of the VC_SA char can be explained by (i) the migration of these elements towards the surface [38] and (ii) the increased concentration of inorganics in the bulk of the char due to carbon burn-off, as confirmed by the AAS analysis detailed in Section 3.1.1.

The EDS analysis confirmed the successful removal of inorganic species from the VC_HCl sample, which contained significantly lower concentrations of Ca, K, and Mg compared with the other samples. Only Si and Cl appeared to persist on the surface of VC_HCl. The presence of Si can be explained by its poor solubility in acid, while the presence of Cl was most likely a consequence of the acid wash treatment, during which Cl^- ions bound to the carbon surface and were not removed by rinsing the char with deionised water. Cl was also present in a small concentration (<0.5 wt.%) in the VC and VC_SA samples, but among the spent chars, only VC_HCl_50N had traces of Cl on the surface. The lack of Cl on the spent samples suggests that the high temperature caused the desorption of this element.

The SEM micrographs correlated well with previously published images of wood char [14,37,39], as illustrated by the selected SEM images presented in Fig. 5. The VC exhibited a fibrous, anisotropic structure typical of softwood, which was evidently preserved in the charred material (Fig. 5a). Most of the EDS scans revealed that AAEM were dispersed across the surface of the chars. In most cases, these elements could not be recognised visually in the SEM micrograph due to their small size and good dispersion. Only a few round-shaped irregular clusters of inorganics, as described by Fuentes-Cano et al. [39], were visible (Fig. 5b). On the surface of VC_HT, agglomeration and sintering of inorganics were observed, as shown in Fig. 5c. This phenomenon was similar to that reported by Klinghoffer et al. [14,37] for chars treated with high temperature (1000 °C).

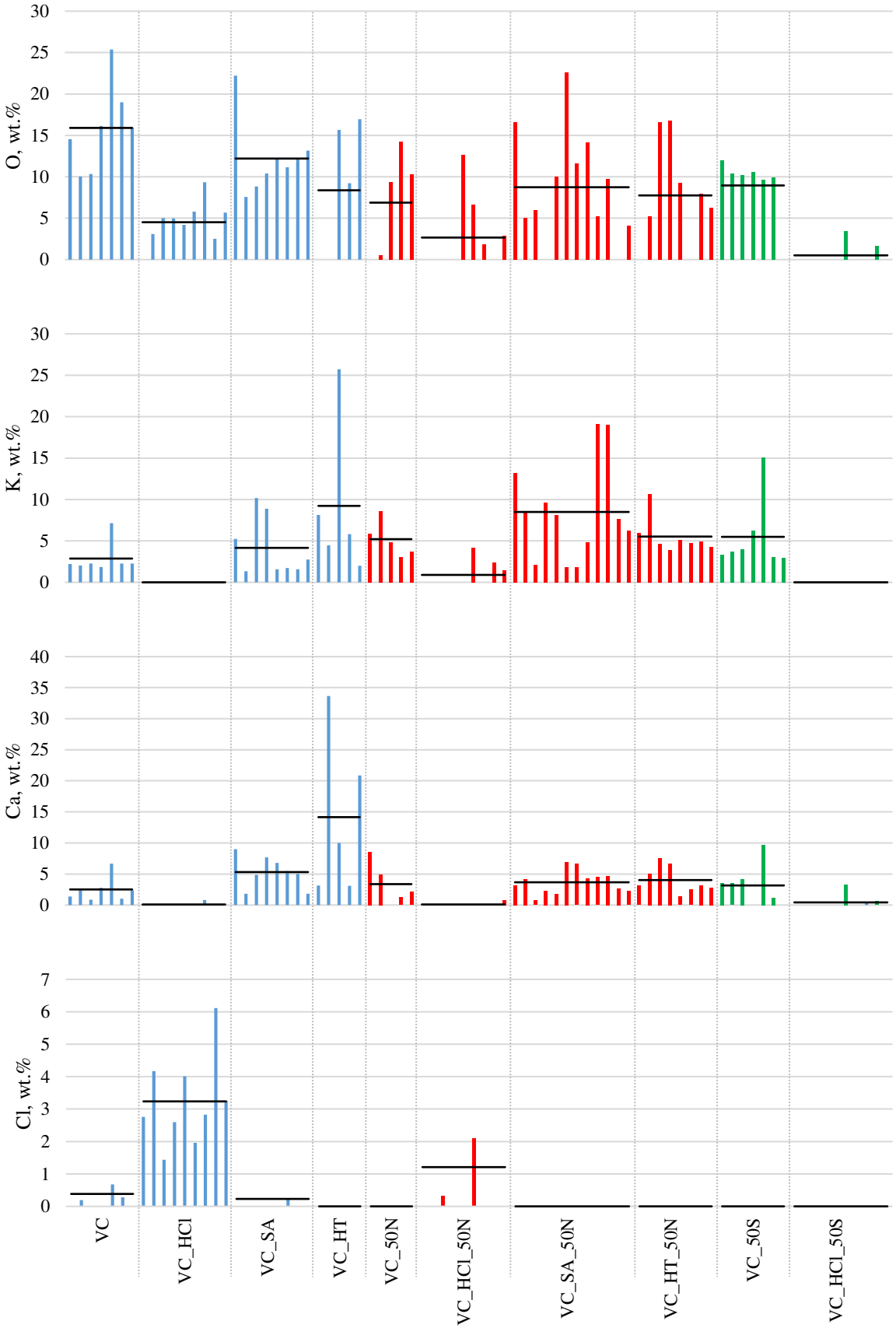
O, wt.%
K, wt.%
Ca, wt.%
Cl, wt.%
VC
VC_HCl
VC_SA
VC_HT
VC_50N
VC_HCl_50N
VC_SA_50N
VC_HT_50N
VC_50S
VC_HCl_50S

406 Fig. 4. The concentration of selected elements determined from SEM-EDS analysis
407 (horizontal lines indicates the average values for each sample)

408

409 The structural changes resulting from the char pre-treatments occurred mainly in the nanoscale,
410 below the resolution of the SEM micrographs. Similarly, no visible modification could be
411 observed following the heterogeneous decomposition of toluene. This can be explained by the
412 relatively short reaction time (50 min). Structural changes caused by cracking reactions on the
413 surface of char have been reported after several hours of char exposure to aromatic compounds.
414 However, the char that was used in those experiments was produced at temperatures below 900
415 °C, thus it may have been less thermally-stable than VC [6,39].

416

a)

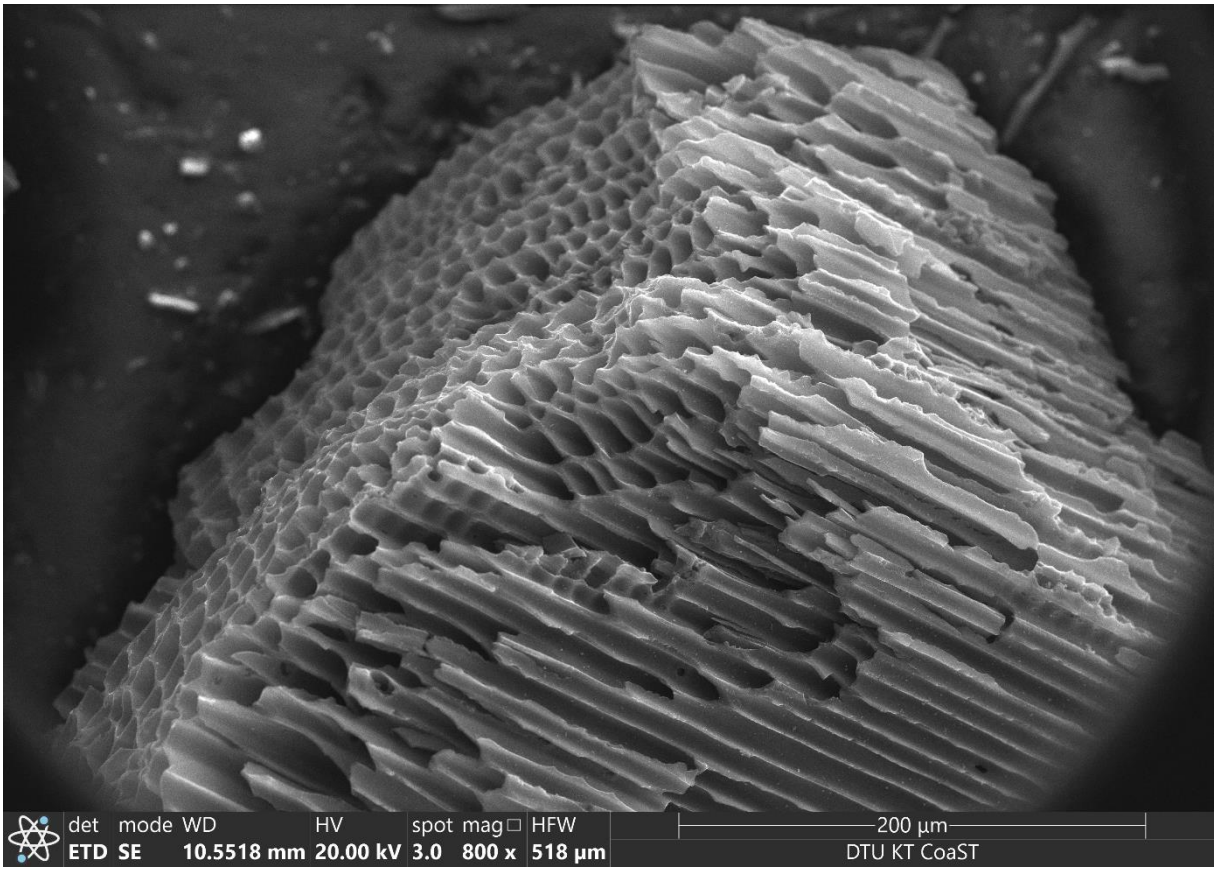

417

418

b)

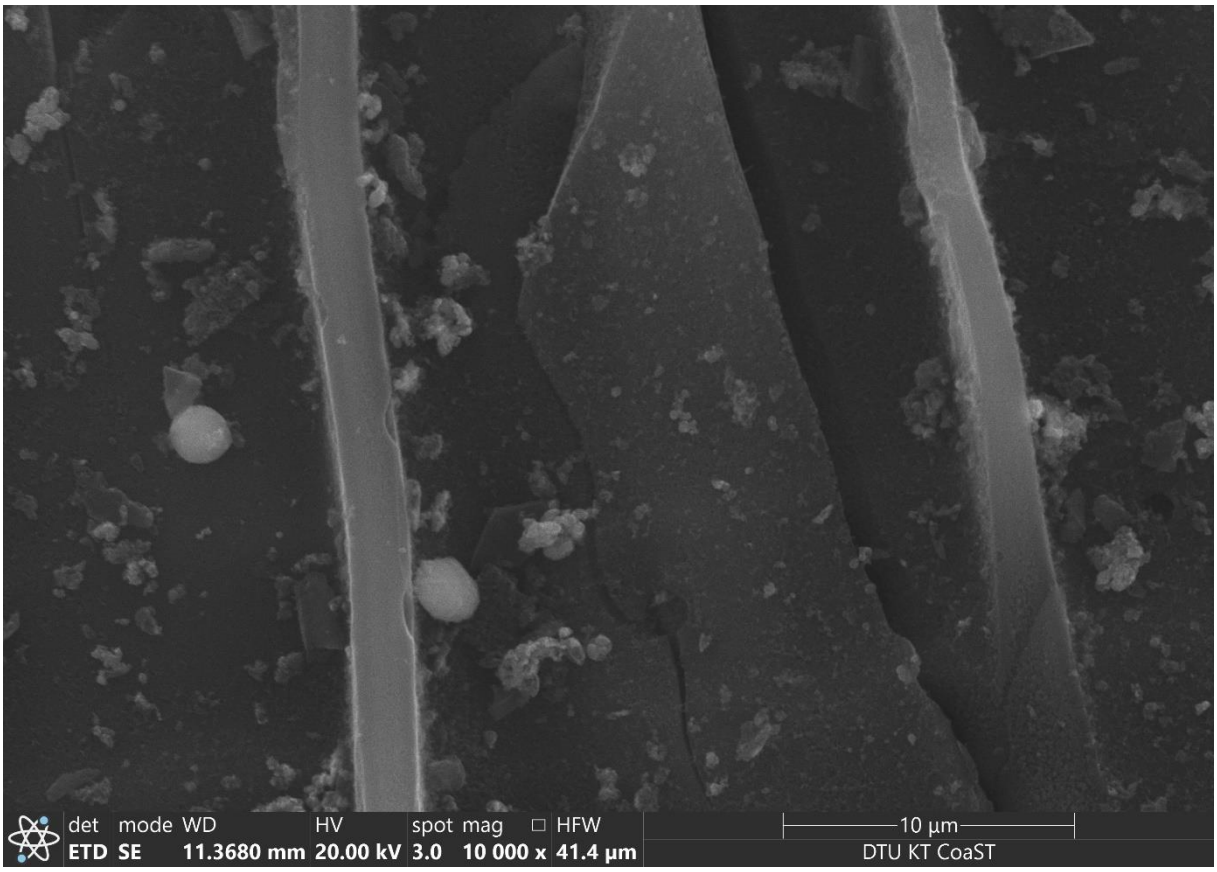
det mode WD HV spot mag HFW
ETD SE 11.3680 mm 20.00 kV 3.0 10 000 x 41.4 µm
10 µm
DTU KT CoaST

419

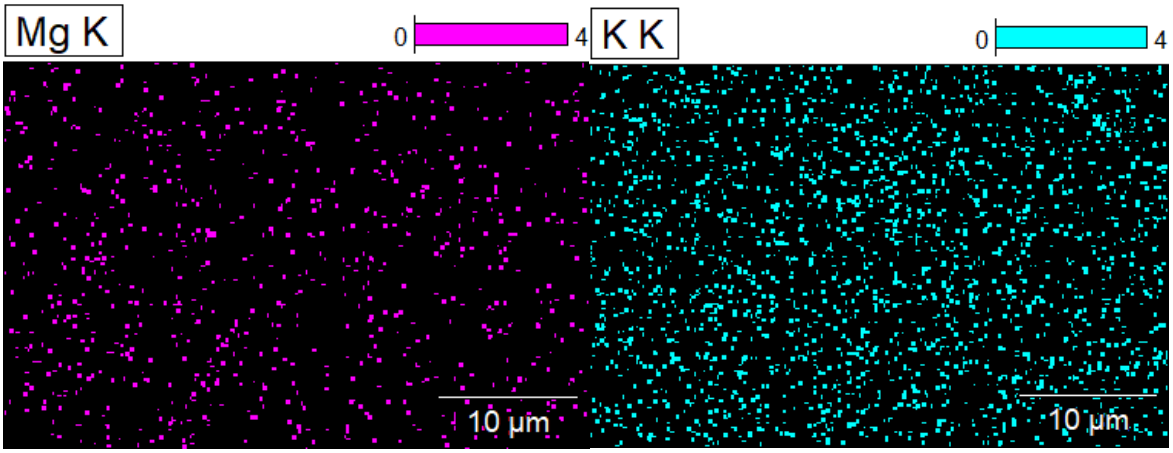
Mg K
0
4
K K
0
4
10 µm
10 µm

420

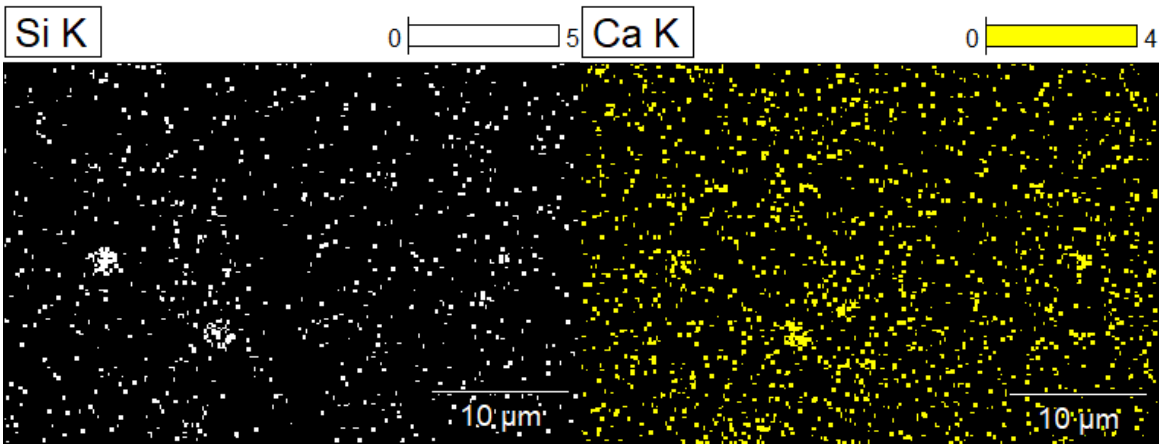
Si K
0
5
Ca K
0
4
10 µm
10 µm

421

c)

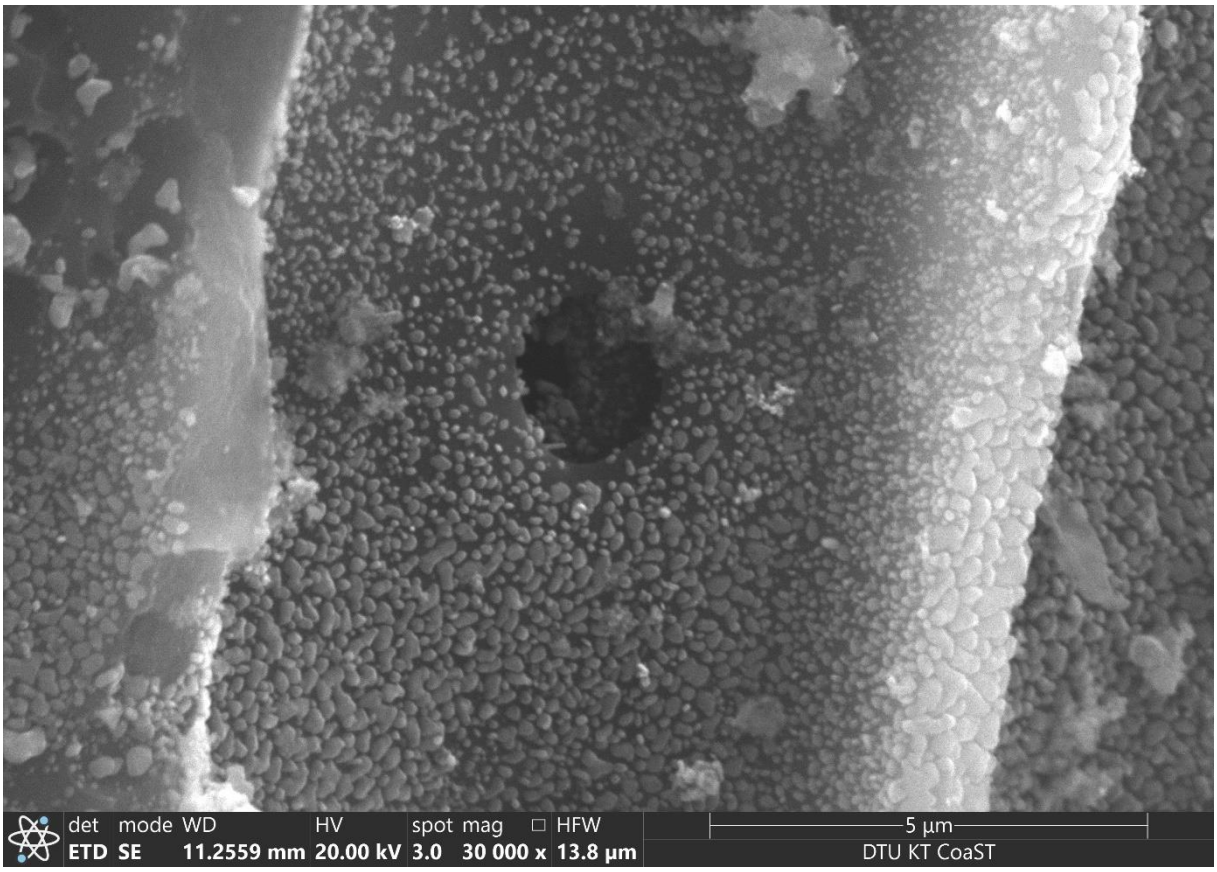

422

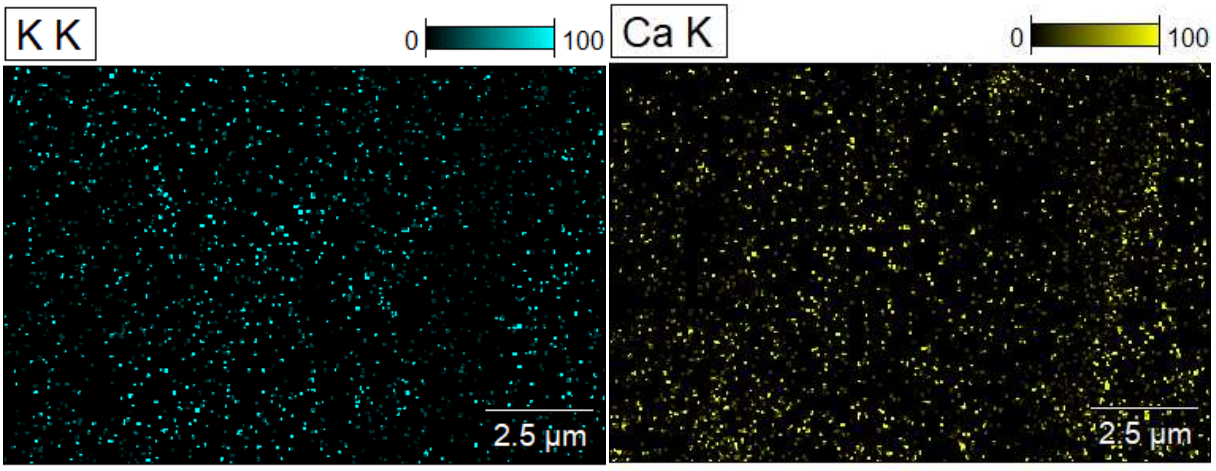

423

424 Fig. 5. SEM micrographs of the VC chars: (a) an anisotropic char grain of untreated VC; (b)
425 cluster of inorganics (Ca and Si) on the surface of VC_SA_50N; (d) inorganics' migration
426 towards the surface and sintering of the VC_HT char

427

428

3.1.3. Surface functional groups

The chemistry of the char surface was examined using ATR-FTIR to verify the effect of the pre-treatments on the surface functional groups and evaluate potential correlations between the functional group content and the catalytic performance of the different materials. The spectra of fresh chars are presented in Fig. 6, and the results for the spent chars are provided in the Supplementary Information. The relatively weak absorption at high wavenumbers suggested insignificant amounts of hydroxyl groups or aliphatic structures in the examined samples [40,41]; O–H and C–H bending motions would be associated with strong peaks around 3700-3000 and 2900-2800 cm^{-1}, respectively. Instead, the observed bands originate mainly from the vibrations of aromatic structures and various carbon-oxygen bonds.

Four characteristic absorption regions can be distinguished in the spectrum of VC, specifically, sharp bands at 1566, 1427, and 874 cm^{-1} and increased intensity in the fingerprint region between 1300-900 cm^{-1}. The sharp bands are most likely related to the aromatic rings in the char. The carbon-oxygen bonds in structures with pronounced resonance effects (i.e., where the energy of the bond is between that of a single and a double bond) may be also responsible for the absorption at 1566 cm^{-1} and 1427 cm^{-1}, e.g. the asymmetric $\nu_{as}(CO_2^-)$ and the symmetric $\nu_s(CO_2^-)$ stretching of carboxylates, respectively [42,43]. The band at 874 cm^{-1} is indicative of one predominant substitution pattern in the aromatic structures, which involves only one or two neighbouring H atoms bound to the ring [41]. The increased absorption in the fingerprint region between 1300-900 cm^{-1} can be attributed to the overlapping frequency ranges for the vibrations of single C–O bonds in various conformations, such as ethers and esters, as well as C–C bonds in the carbonaceous matrix of the char. Moreover, a weak, broad band around 3700-3000 cm^{-1} suggests a small amount of lattice water or a trace amount of hydrogen-bonded hydroxyl groups. The increased absorption around 2600-1700 cm^{-1} may indicate the presence of some

C=O groups, such as lactones or quinones, or it may result from the overtones of aromatic ring stretching.

All the treatments applied to VC decreased the char absorption in certain regions, indicating that the pre-treatments caused a significant loss of surface functionalities. Acid washing (VC_HCl) led to almost complete disappearance of the 1427 and 874 cm^{-1} bands, indicating the destruction or rearrangement of carboxylate ions and changes in aromatic rings substitution, respectively. Steam activation (VC_SA) had a similar effect, with an additional decrease of the 1560 cm^{-1} band and slightly diminished absorption in the fingerprint area. The spectrum of the thermally-treated char (VC_HT) was drastically flattened, suggesting major decomposition of the surface functionalities. Acid washing most likely protonated carboxylates and changed the substitution pattern in aromatic structures, thus shifting the sharp 874 cm^{-1} band towards 800 cm^{-1}. Carboxylates thermally decompose around 440 °C [44], so it is possible that they were released from the char surface during heating under an inert atmosphere, or even in the presence of steam, despite its oxidising effect, thus removing the 1427 cm^{-1} band from the VC_HT and VC_SA char spectra. The depleted absorption of the VC_SA sample, compared with VC, suggests that the atmosphere in the second stage of the Viking gasifier where the untreated char was created, was more reactive than the steam pre-treatment conditions. Therefore, although the applied steam activation enhanced the surface area development of the VC_SA char (discussed further in Section 3.1.4), it was not sufficient to maintain the O-containing functionalities of the VC.

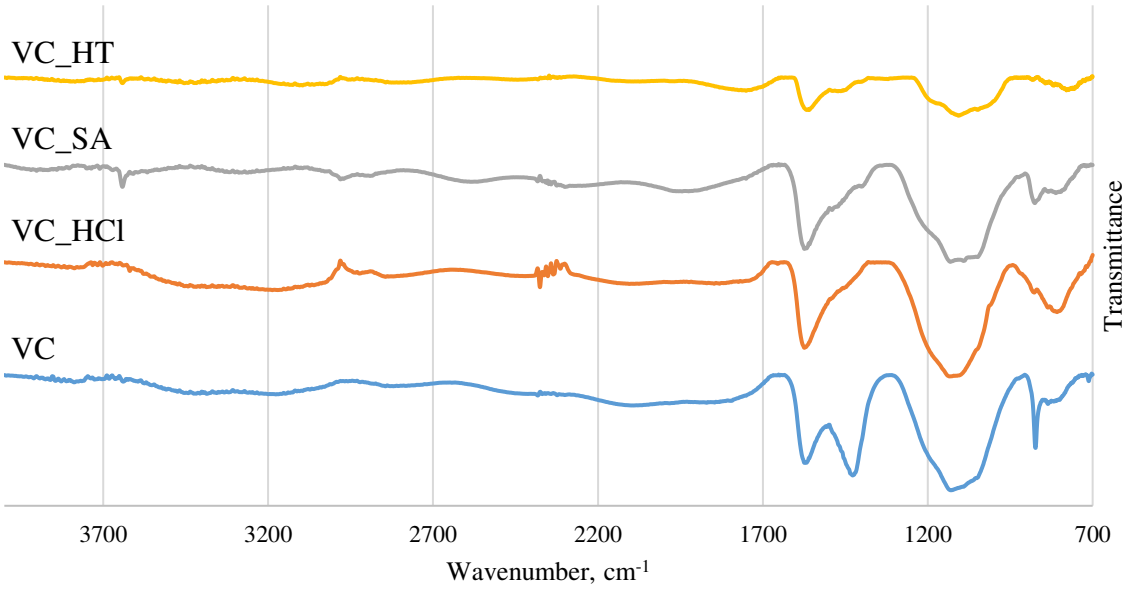

Fig. 6. ATR-FTIR spectra of the fresh chars: untreated VC, acid-washed VC_HCl, steam-activated VC_SA, and thermally-annealed VC_HT

3.1.4. Surface area and pore size distribution

The structures of the fresh and spent char samples were examined by measuring the N_2 adsorption at 77 K and the CO_2 adsorption at 273 K. The adsorption branches of both isotherms were then combined to obtain the pore size distribution (PSD), presented in Fig. 7, using the 2D-NLDFT model. All samples contained significant quantities of micropores, among which, two characteristic groups could be distinguished, namely, ultramicropores (<7 Å [45]; here, 3-5 Å) and supermicropores (10-20 Å). Additionally, some mesopores (>20 Å) with a wide variety of sizes were observed in all PSD plots. The incremental area of the ultramicropores in the VC reached 70 m^2/g, and these structures were preserved following acid wash (VC_HCl) and thermal pre-treatments (VC_HT), although steam activation decreased the area to 60 m^2/g (VC_SA). The main peak in the supermicropores' distribution curve (at 11 Å) increased by 10 m^2/g due to acid washing and by 20 m^2/g due to steam activation, whereas thermal annealing

490 resulted in a 10 m^2/g decrease. The area of larger supermicropores and mesopores was similar
491 for all samples, except the VC_SA char. The consumption of carbon during steam gasification
492 has a pore-widening effect [46], which was likely responsible for the decrease in
493 ultramicroporous area and the increase in the supermicroporous and mesoporous area of the
494 steam-activated material. High-temperature annealing resulted in pore collapse and/or sintering,
495 thereby diminishing the area of supermicropores in VC_HT. In contrast, the removal of some
496 labile carbon species during the acid wash may explain the increased microporosity of the
497 VC_HCl char.

498 Heterogeneous toluene conversion over the catalyst surface results in coke deposition inside
499 the pores, thus decreasing the surface area of the material. In general, micropores are relatively
500 more prone to blockage and deactivation [6,29,47]; therefore, more mesoporous structures
501 typically have higher longevity. Indeed, the PSD in the spent chars recovered after 50 min of
502 catalytic toluene conversion in an inert atmosphere revealed a significant decrease in their
503 supermicroporous areas. In particular, VC_50N and VC_HT_50N suffered the most severe
504 deactivation and their pores between 10-15 Å became completely filled with coke. In the
505 slightly more resilient VC_HCl_50N and VC_SA_50N chars, residual amounts of pores with
506 sizes of ca. 14 Å were preserved. This observation suggests that supermicropores were
507 progressively filled from the smallest to the largest, during coke deposition. Interestingly, the
508 surface area contained in ultramicropores did not diminish in the spent samples. Since these
509 pores are smaller than the kinetic diameter of toluene (5.85 Å [48]), they likely did not
510 participate in toluene conversion. Their presence in the PSD of spent chars suggests that the
511 entrance to those pores was not blocked by deposited coke, so it is plausible that they were not
512 embedded in the supermicropores, but rather, were directly accessible from the meso and
513 macropores, which were not completely filled with coke. The observed changes in the pore
514 distribution following catalysis suggest that (i) the coke deposition occurred primarily in the

515 micropores and (ii) the ultramicroporous structures did not participate in the catalytic
516 conversion of toluene, so they were resistant to deactivation. The general exclusion of
517 micropores from catalysing tar conversion because of diffusional limitations was previously
518 reported by Fuentes-Cano et al. [39]. In this study, the inclusion of CO_2 adsorption
519 measurements in the PSD calculation provided additional information on the ultramicropores,
520 allowing the conclusion that only the smallest micropores did not contribute to toluene
521 conversion, and the critical size of the pores participating in the conversion correlate well with
522 the kinetic diameter of the compound. The results of the 2D-NLDFT model also suggested that
523 micropores that are too narrow for toluene did not get blocked by the coke deposited at their
524 entrance, but remained unaffected by both the toluene conversion and the deactivation
525 processes. Verification of this proposal requires further investigation, e.g., using additional
526 samples to determine if discussions of biochar microporosity should distinguish between
527 ultramicropores and supermicropores.

528 During toluene conversion in the presence of steam, the gasification of the char and the
529 deposited coke occurred, thus the pore structure was preserved. This phenomenon was more
530 pronounced in the case of VC, which demonstrated greater reactivity than VC_HCl during the
531 gasification, as discussed further in Section 3.2. Most of the original pores were preserved in
532 the spent VC_50S char, and the slight decrease in the microporous area was most likely the
533 result of the pore-widening effect of carbon consumption during reactions with steam. In
534 contrast, since the VC_HCl char was more resistant to gasification, the beneficial role of steam
535 was limited in this case. The VC_HCl_50S char had fewer micro and mesopores, although the
536 pore blocking was less intense compared with the tests under an inert atmosphere
537 (VC_HCl_50N). Toluene reforming with VC_HCl char confirmed that the coke deposition
538 occurred preferentially in the smaller supermicropores (~11 Å), as the area corresponding to
539 these structures decreased the most following catalysis.

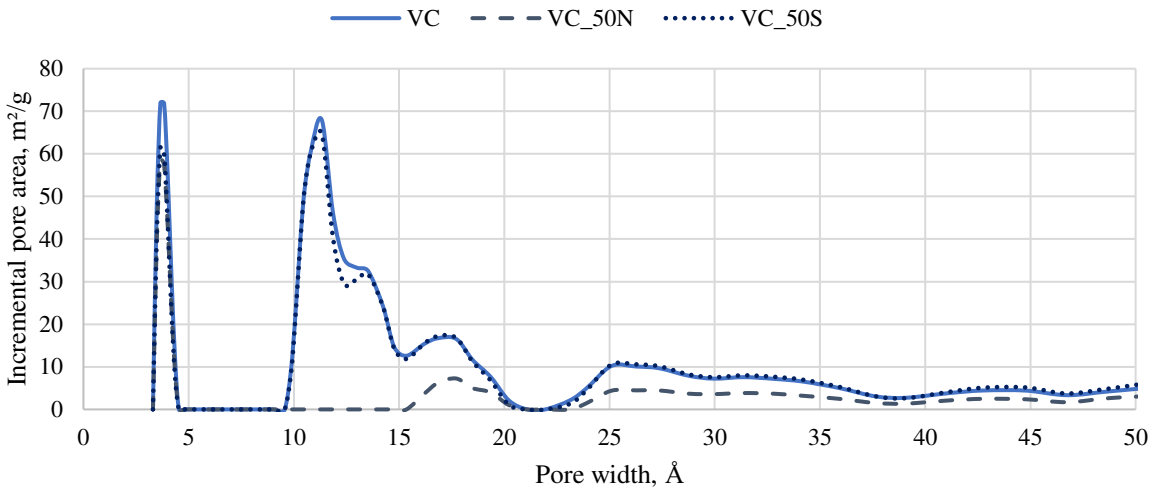

540

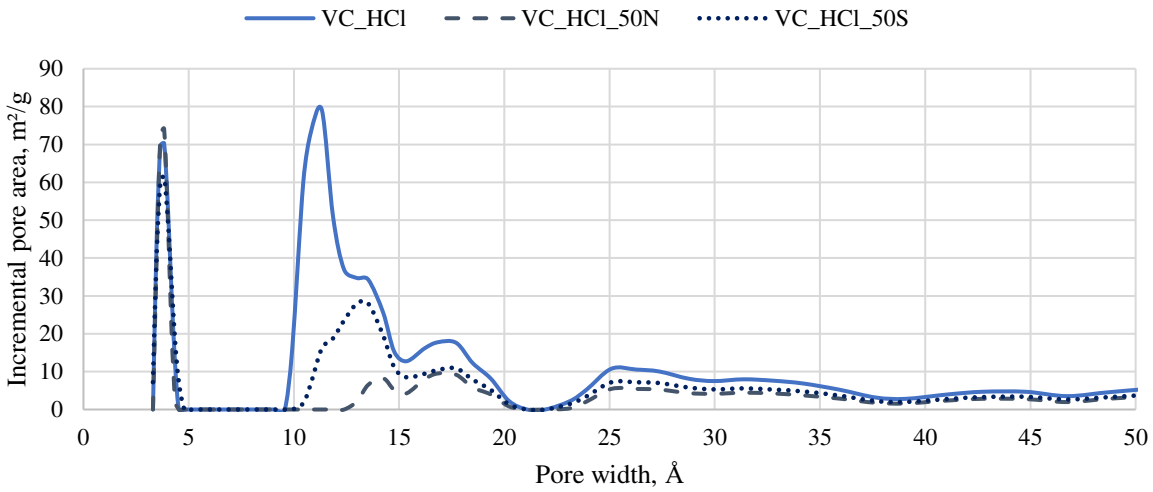

541

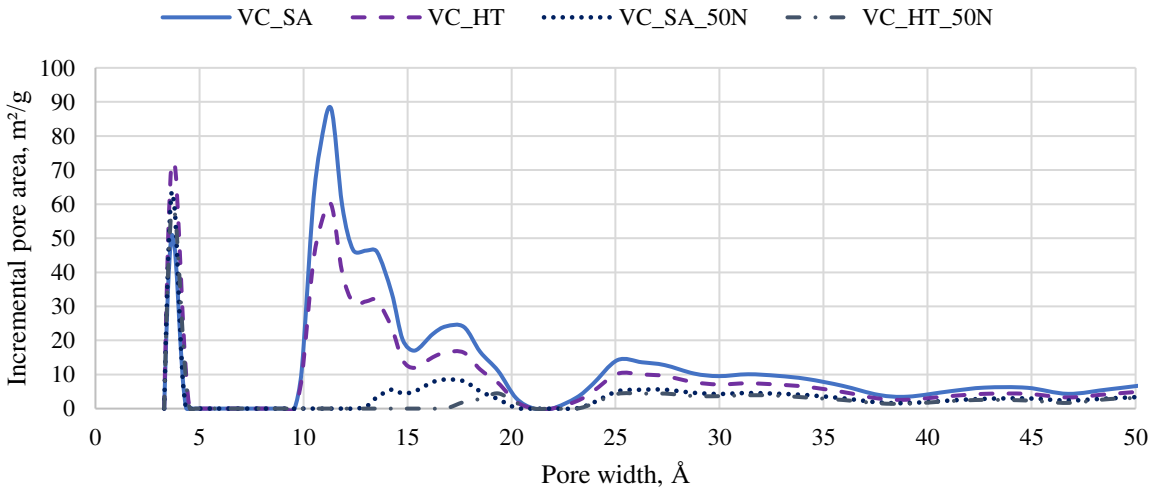

542

543 Fig. 7. NLDFT pore size distributions calculated from the combined results of N_2 and CO_2

544 adsorption

545 The total surface area of the samples was calculated using a BET model based on the N_2
546 adsorption isotherm (Fig. 8). These data were also used to estimate the area of the micropores
547 with the t-Plot method. The BET model was also applied to the CO_2 adsorption data; the
548 calculated surface area accounts for micropores up to approximately 10 Å. It was determined
549 that VC had a very high surface area, comparable with that of activated carbons. Both acid wash
550 and steam activation effectively increased the surface area, as a result of the removal of
551 inorganics and carbon burn-off, respectively. In contrast, the heat treatment decreased the BET-
552 determined surface area due to pore collapsing.

553 Coke deposition during the pyrolytic toluene conversion significantly diminished the total
554 surface area of all four examined spent chars. Conversely, the area of micropores determined
555 by the CO_2 measurements was only slightly diminished; most of these pores were the
556 ultramicropores (<5 Å), which were not affected by the coke deposition according to the PSD
557 results. It should be noted that the microporous area calculated with t-Plot method was similar
558 to that derived from CO_2 adsorption for the fresh chars. However, there was a large discrepancy
559 between the t-Plot and CO_2 adsorption results from the spent char analysis. It is plausible that
560 the coke deposit effectively limited N_2 diffusion into the smallest pores, while the CO_2 was still
561 able to enter those structures. Therefore, the assessment of the microporous carbons with CO_2
562 adsorption proved to be crucial for understanding the structural changes in the char during
563 deactivation with coke deposition. Furthermore, these results confirmed that the incorporation
564 of data from the CO_2 measurement into the PSD calculation is necessary to obtain a realistic
565 distribution of the ultramicropores. The microporous areas determined from t-Plot and CO_2 data
566 were consistent for the material recovered after steam reforming of toluene over the VC because
567 the structure of the VC_50S sample was well-preserved. However, for the partially coke-
568 covered VC_HCl_50S char, the t-Plot method again underestimated the area of the micropores
569 by not accounting for the ultramicropores.

570 Since the ultramicropores did not participate in toluene conversion, the term "useful surface
571 area" of the char was introduced, and this value was determined as the integrated area under the
572 PSD plot for the pores wider than the toluene kinetic diameter (5.85 Å). This surface parameter
573 was further utilised to correlate the catalyst surface development with the toluene conversion,
574 as reported in Section 3.4.

575

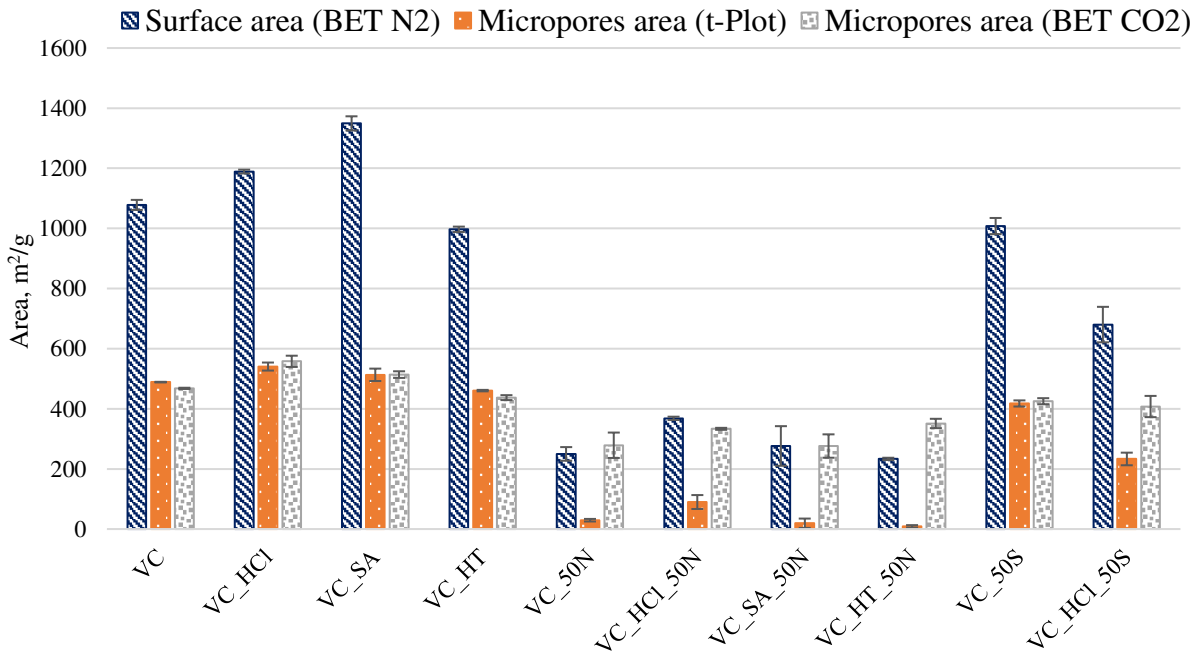

576

577 Fig. 8. The chars' surface areas calculated with a BET model based on N_2 and CO_2 adsorption
578 data, and the microporous area calculated with a t-Plot model applied to the N_2 measurements

579

580 **3.2. Gasification reactivity of the chars**

581 The reactivities, R_{50}, of the untreated and modified chars were analysed to evaluate the influence
582 of the changes in the surface area and inorganic content on the rate of char gasification with
583 CO_2. In addition to the TGA measurements at the temperature corresponding to the toluene

reforming tests (800 °C), TGA runs were performed at 850 and 900 °C to determine the kinetic parameters for the VC and VC_HCl samples. These parameters were employed to compare the gasification of the untreated char catalysed with inherent inorganics, with the non-catalytic gasification of the acid-washed material. The kinetic analysis was carried out as described in Section 2.3, and the obtained R_{50} values are presented in Fig. 9. The R_{50} values from the VC and VC_HCl gasification at 800 °C differed by an order of magnitude, and at higher temperatures the discrepancy between the chars become even more pronounced. While increasing the temperature from 800 °C to 900 °C, the reactivity increased from 0.56×10^{-3} s^{-1} to 3.75×10^{-3} s^{-1} and from 0.07×10^{-3} s^{-1} to 0.22×10^{-3} s^{-1} for the VC and VC_HCl chars, respectively. It can be expected that removing char inorganics during the acid wash and the consequent lack of AAEM catalytic effects resulted in the VC_HCl char's poor sensitivity to temperature changes. The 100 °C rise in the reaction temperature increased the reactivity of the VC char over six times and increased the VC_HCl char's reactivity only three times, indicating the higher activation energy of the VC char within the examined temperature range (Table 1).

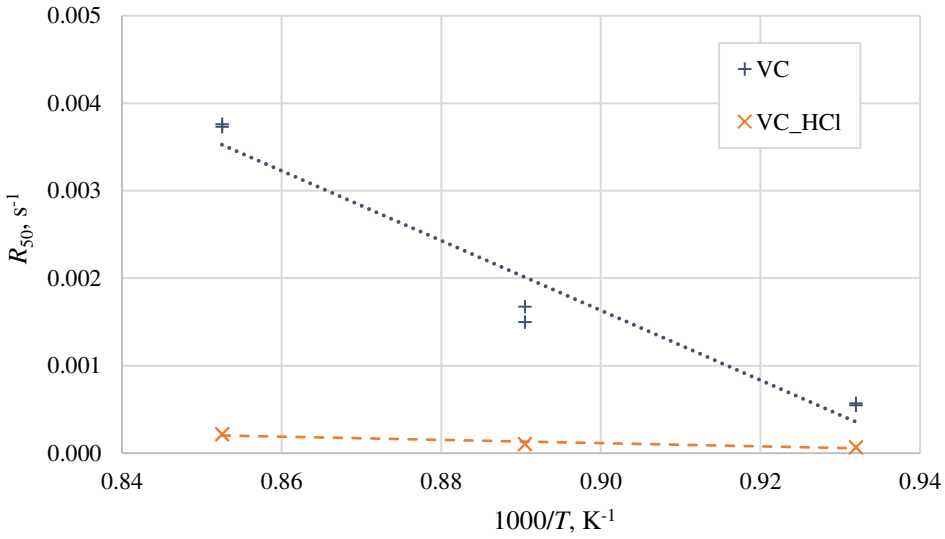

Fig. 9. Untreated (VC) and acid-washed (VC_HCl) char reactivity as a function of the temperature of the CO_2 gasification

602 Table 1. Kinetic parameters of untreated (VC) and acid-washed (VC_HCl) char gasification
603 calculated based on the reactivities determined at 800, 850 and 900 °C

	E, kJ·mol^{-1}	k_0, bar^{-1}·s^{-1}	R^2
VC	199	3.61E+06	0.997
VC_HCl	119	5.42E+01	0.964

604

605 In addition to the fresh chars, the spent materials recovered after 50 min of toluene conversion
606 were also analysed in terms of their reactivity during CO_2 gasification at 800 °C in order to
607 examine the influence of the coke formation and steam activation that occurred during these
608 tests. The R_{50} values of fresh and spent chars are compiled in Table 2.

609

610 Table 2. Overview of the reactivity (R_{50}) of fresh and spent char samples

	Fresh	Spent 50 min in N_2	Spent 50 min in steam/N_2
	$R_{50}\times10^3$ (1/s)	$R_{50}\times10^3$ (1/s)	$R_{50}\times10^3$ (1/s)
VC	0.56 ± 0.02	0.46 ± 0.04	0.55 ± 0.03
VC_HCl	0.07 ± 0.01	0.06 ± 0.01	0.06 ± 0.01
VC_SA	0.94 ± 0.12	0.68 ± 0.01	
VC_HT	0.69 ± 0.04	0.45 ± 0.01	

611

612 The pre-treatments applied to VC significantly affected its gasification reactivity. In particular,
613 acid washing drastically decreased R_{50}. This result confirmed the important role that inorganics
614 play in determining the gasification reactivity of chars. In contrast, the steam activation and

heat treatment effectively increased R_{50}. In the case of VC_SA, this was because of the increased surface area and AAEM content. In the case of VC_HT, this may be the result of metals rising to the surface following high-temperature treatment [37].

The pyrolytic conversion decreased the R_{50} values of VC, VC_SA, and VC_HT. The toluene-derived coke was deposited on the char surface, thereby hindering the access to smaller pores (decreasing the surface area) and covering the AAEM species. This also significantly reduced the number of accessible active sites on the char surface, thus inhibiting the reactivity of spent chars. Steam reforming of toluene over the VC char maintained the reactivity of the char due to its continuous re-activation with steam.

No significant differences between the R_{50} values of fresh and spent VC_HCl chars were observed. Since most of the AAEM species were already removed from the sample during the pre-treatment, the coke layer did not have a deactivating effect, while the steam-activating effect was negligible due the generally poor reactivity of the VC_HCl sample. The comparison of the mass loss curves of the fresh and spent VC and VC_HCl chars, presented in Fig. 10, confirmed that the gasification of the VC char that was spent during toluene pyrolysis was slower than that of fresh VC and the sample recovered after steam reforming. Interestingly, the mass loss curves for both spent VC_HCl chars were slightly less rapid than the fresh material. It is possible that although the toluene conversion did not affect the reactivity of the char, the char became more stable due to the high-temperature exposure during the conversion experiments. The difference between the shapes of the mass loss curves of VC and VC_HCl chars should be also noted. It is generally acknowledged [49] that the rate of biomass char gasification increases with the char burn-off due to the increasing concentration of inorganics. This behaviour resulted in the curved mass loss plots obtained for fresh and spent VC chars. Because of the lack of inorganics in the VC_HCl samples, the mass loss functions of these acid-washed materials were linear, as no AAEM densification effect occurred.

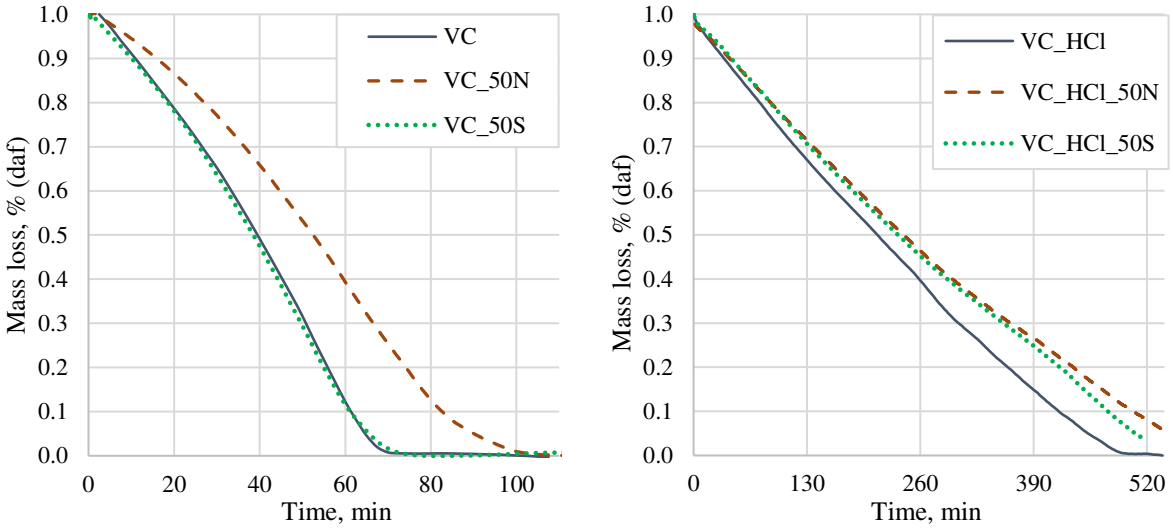

640

641 Fig. 10. Mass loss curves during CO_2 gasification of the untreated (VC) and acid-washed
642 (VC_HCl) chars, and the chars recovered after 50 min of toluene conversion in pure nitrogen
643 (50N) or 15.5 vol.% of steam (50S)

644

645 **3.3. Catalytic effect of the chars on toluene decomposition**

646 The toluene conversions (η_T) obtained from the experiments summarised in Fig. 1 are reported
647 in Table 3. The relatively high values of η_T confirm the good performance of this char for the
648 heterogeneous conversion of toluene. The values of η_T are similar to values reported in
649 literature for toluene conversion over char under similar conditions [35,50]. In addition, in N_2
650 atmosphere, all the samples exhibited reduced conversion over time due to coke deposition and
651 blocking of active sites. This mechanism is the same as that which reduced the gasification
652 reactivity of spent chars.

653

654

655 Table 3. Toluene conversion $(\eta_T, \%)$ over the tested chars under an inert N_2 atmosphere and in
656 the presence of steam

Atmosphere:	N_2	N_2	Steam/N_2
Feeding time:	30 min	50 min	50 min
VC	75 ± 2	67 ± 1	74 ± 2
VC_HCl	79 ± 2	72 ± 1	75 ± 1
VC_SA	88 ± 4	78 ± 1	
VC_HT	70 ± 1	60 ± 1	

657

658 The different chars varied significantly in their catalytic performances. It is especially
659 interesting to note that the performance of the VC_HCl char was not impaired by the removal
660 of inorganics. On the contrary, its efficiency for toluene pyrolytic conversion was slightly
661 higher than the untreated VC char, especially for the 50 min runs, where the toluene conversion
662 increased from 67 % to 72 % as a result of this pre-treatment. The steam activation increased
663 the surface area of VC_SA and significantly enhanced its catalytic affinity, while the degraded
664 surface structure resulting from the thermal treatment of VC_HT inhibited its performance.

665 These results suggested that the metals inherently present in VC did not play any major role in
666 the heterogenous conversion of toluene. The enhanced performance of the VC_HCl char may
667 be related to the observed increase in its surface area or the protonation of the active sites. The
668 role of AAEM during volatile-char interactions was further investigated with steam reforming
669 tests. Under oxidising conditions, the char surface is involved in two types of reactions: (1) the
670 heterogeneous toluene conversion to coke and (2) the solid carbon gasification. As suggested
671 by the previous studies [9,36], these two reactions occur independently, and the ratio of their
672 individual rates determine if the catalyst loses or maintains its activity throughout the reforming
673 process. Thus, steam introduction should result in the solid carbon gasification, which was not
674 the case in the pyrolytic runs. Therefore, in this mode, despite no effect of AAEM on
675 heterogenous toluene conversion, their catalytic effect on carbon gasification was expected to

676 influence the reforming process in an indirect way, i.e. by enhancing char/coke gasification.
677 The drastic difference in the R_{50} values of the VC and VC_HCl chars was expected to offset the
678 balance between the rates of the toluene-derived coke formation and char consumption. Indeed,
679 the introduction of steam resulted in an increase in toluene conversion from 67 % to 74 % for
680 VC and only from 72 to 75 % for VC_HCl sample. This observation suggests that, although
681 heterogeneous conversion of toluene was not directly affected by the presence of inorganics,
682 they indirectly contributed to the increased efficiency of the conversion over VC by enhancing
683 gasification of this char and thus prolonging its activity.

684 The surface functionalities identified by FTIR did not appear to play an important role in the
685 decomposition of toluene. All applied pre-treatments decreased the quantity of O-containing
686 groups on the char surface, although different trends in the η_T values were observed for different
687 modified materials.

688 The role of steam in the toluene reforming process was confirmed by analysing the released
689 gases presented in Fig. 11. The pyrolytic conversion of toluene yielded only H_2 and CH_4 (see
690 Supplementary Information); however, during the steam reforming process, CO_2 and CO
691 originating from the solid carbon gasification were also detected. Greater amounts of carbon
692 oxides and H_2 were released during the tests with VC, relative to VC_HCl, thus confirming that
693 the rate of the char/coke reaction with steam was faster when inorganics were present in the
694 catalyst. Some studies [51] have described the significant influence of the inherent AAEM
695 species on the water-gas shift reaction (i.e., $CO + H_2O \rightarrow CO_2 + H_2$), leading to increased
696 selectivity towards CO_2 during catalytic gasification [19], which might explain the particularly
697 high CO_2 yield during the test with the VC char. The linear mass loss of the VC_HCl char
698 registered during TGA tests revealed a constant gasification rate for this material. Additionally,
699 the similar reactivities of the spent and fresh samples suggested that the coke layer formed
700 during toluene conversion did not inhibit the gasification of the catalyst bed. Thus, the CO

release directly from the heterogenous water-steam reaction (i.e., via $C + H_2O \rightarrow CO + H_2$) was constant throughout the steam reforming experiment with VC_HCl. In contrast, the toluene-derived coke was less reactive than the AAEM-rich VC char, as revealed by the lower R_{50} value for the spent, coke-covered VC char (0.46×10^{-3} s^{-1}) recovered after pyrolytic toluene conversion relative to the R_{50} of the fresh VC char (0.56×10^{-3} s^{-1}). Thus, as the reaction proceeded, the coke contributed more and more to the total amount of solid carbon interacting with steam, so the rate of gasification and the CO yield both decreased. The continuous deposition and steam consumption of the coke inhibited the gasification of the char bed, but also helped preserve the reactivity of the VC char recovered after the reforming test (0.55×10^{-3} s^{-1}). The non-catalysed gasification has also been correlated with increased CH_4 formation [19], which was observed during toluene reforming over the VC_HCl char in this study.

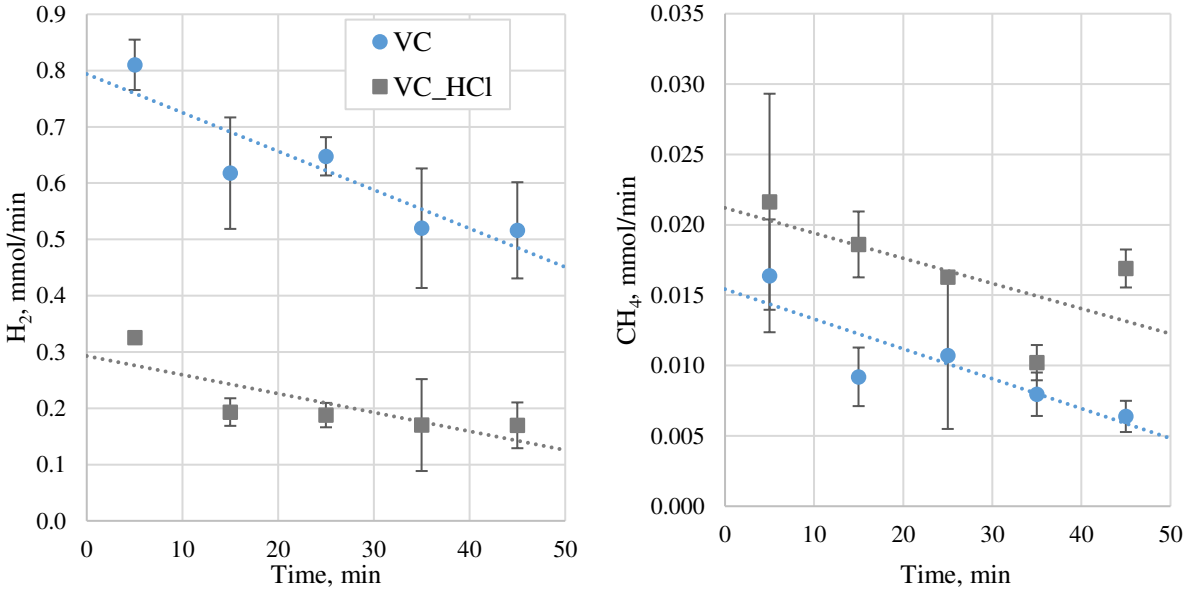

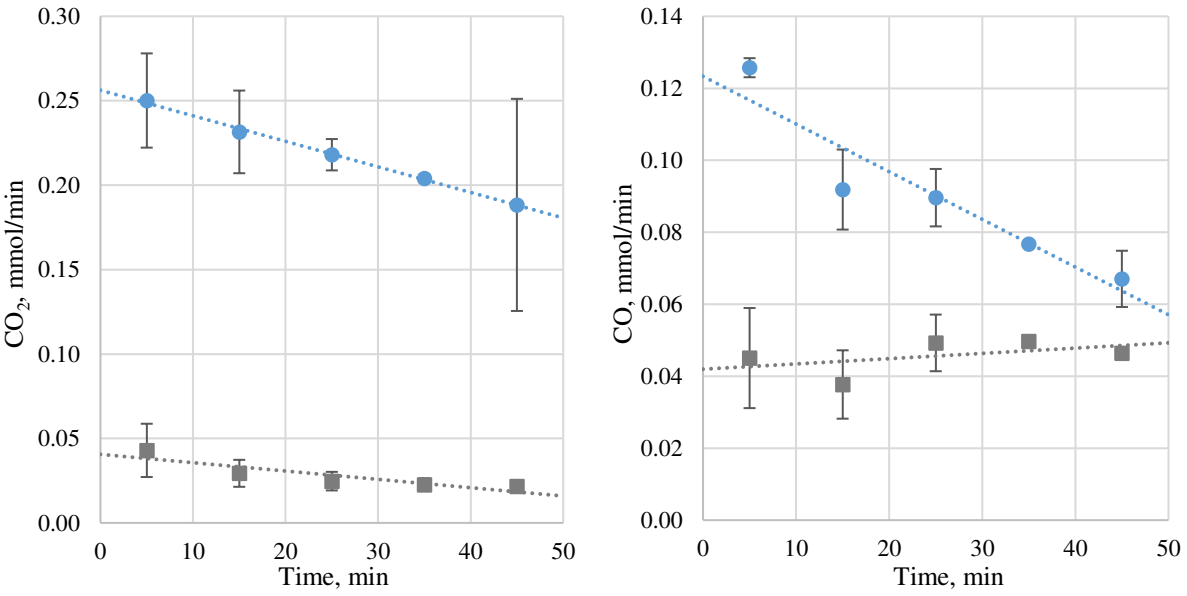

715

716 Fig. 11. Gas evolution during the steam reforming of toluene over the untreated (VC) and acid-
717 washed (VC_HCl) chars

718

719 In addition to the permanent gases, some liquid by-products of toluene conversion were
720 detected (Fig. 12 and Supplementary Fig. S2). The demethylation of toluene resulted in the
721 formation of a substantial amount of benzene. Moreover, some secondary reactions led to
722 methyl substitution either directly on the aromatic ring or on the existing methyl group of
723 toluene molecules, yielding small amounts of xylenes and ethylbenzene. Some of the ethyl
724 groups underwent dehydrogenation to produce styrene. It was previously reported [52] that
725 toluene decomposition to benzene intensifies as the catalyst becomes saturated with coke.
726 Therefore, the selectivity towards benzene formation was lower during (i) pyrolytic toluene
727 conversion over the VC_SA char, which had a higher capacity for coke due to its larger and
728 more mesoporous surface area, and during (ii) steam reforming over the VC char, where the
729 coke was continuously removed by steam gasification, compared with the other chars. The
730 secondary reactions leading to the formation of substituted benzenes formation are also

731 intensified when the catalyst is deactivated. Therefore, larger amounts of these compounds were
732 generated during toluene pyrolysis, compared with steam reforming.

733 The construction of the test rig did not allow for gravimetric assessment of the mass gain/loss
734 of the catalyst bed; therefore, carbon balance was performed to estimate carbon accumulation
735 in the reactor during toluene conversion tests. The amounts of carbon in the liquid and gaseous
736 products, as well as in the unreacted share of toluene are presented in Fig. 13 as a percentage
737 of the amount of carbon fed into the reactor with the toluene. For the pyrolytic tests, where no
738 char/coke gasification occurred, the amount of the fed toluene that was converted into coke can
739 be therefore estimated by difference, as indicated by the grey sections of the VC, VC_HCl,
740 VC_SA, and VC_HT bars. These sections were relatively similar for all examined chars, with
741 the highest coke deposition on the most efficient and most mesoporous sample (i.e., VC_SA),
742 and the lowest coke yield on the least effective char (i.e., VC_HT).

743 Different information can be obtained from Fig. 13 for the toluene reforming tests. In this case
744 a part of the char bed and toluene-derived coke underwent steam gasification. Hence, an
745 unknown share of released gases comprised carbon that was introduced into the reactor with
746 the char bed and not with the fed toluene. Thus, for these experiments, the amount of created
747 coke cannot be calculated from the performed carbon balance. However, results presented as
748 the bars VC_steam and VC_HCl_steam represent the overall change in C content in the reactor
749 that occurred as a result of three concurrent reactions involving the solid carbon: coke
750 formation, coke gasification, and char gasification. The total amount of C released during the
751 steam test with the VC char exceeds the amount fed with the toluene, which suggests that the
752 total amount of coke and char consumed during the reforming process was higher than the
753 amount of the deposited coke. However, it is impossible to determine the proportion of the
754 gasified coke versus the char. Compared with the pyrolytic test, the presence of steam also
755 decreased the amount of coke/char in the bed of the acid-washed VC_HCl char, yet the lower

gasification rate observed for this catalyst did not prevent the accumulation of carbon on its surface. The deactivation of the spent chars was also confirmed by the reduction in their FTIR spectral intensities (see the Supplementary Information); some functional groups remained in the VC char after steam reforming, whereas the spectra of both spent VC_HCl chars and the VC char recovered after pyrolysis were flattened.

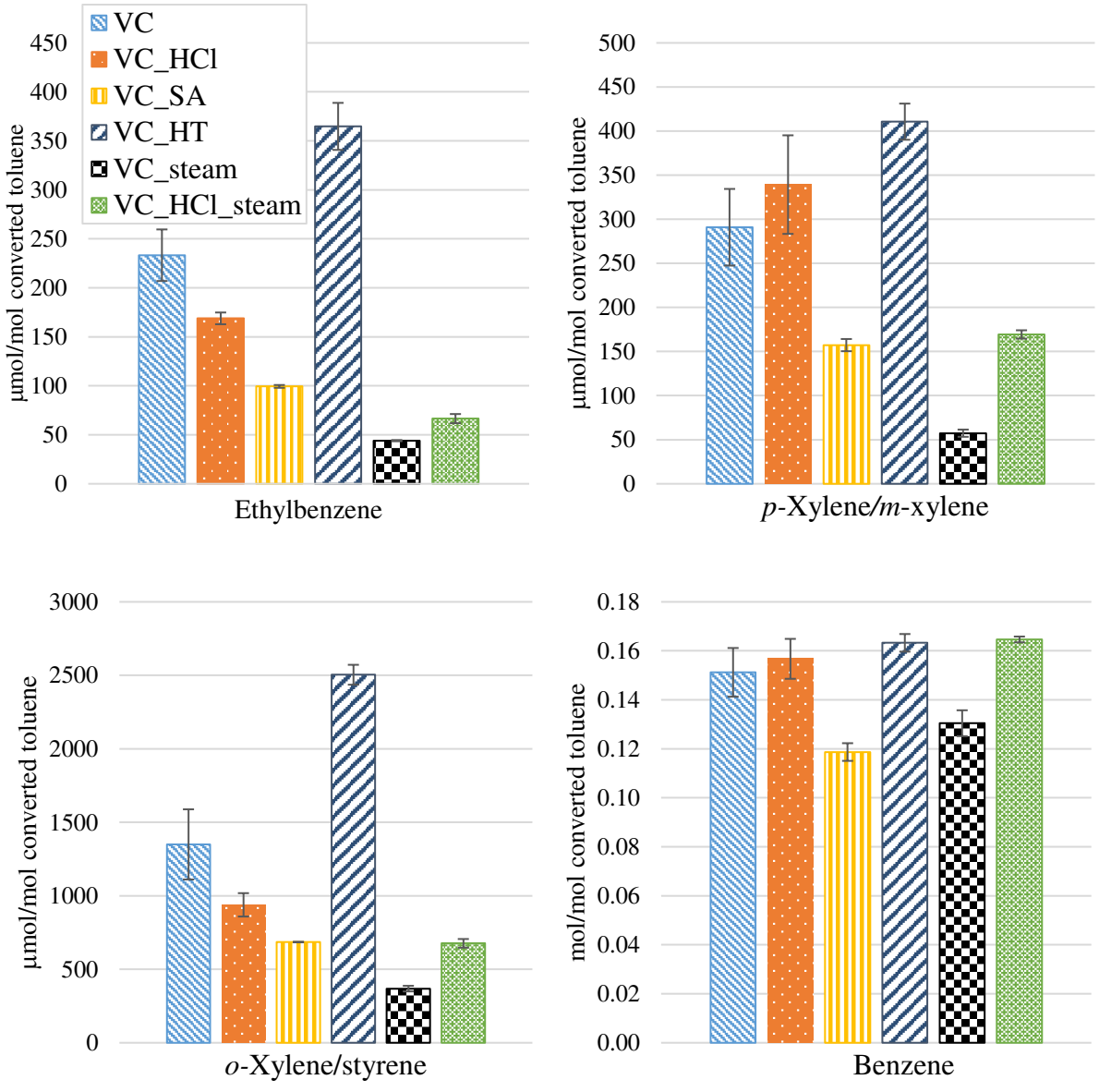

Fig. 12. Relative molecular yields of liquid by-products following 50 min of toluene conversion over the chars under inert (N_2) and oxidising (steam) conditions

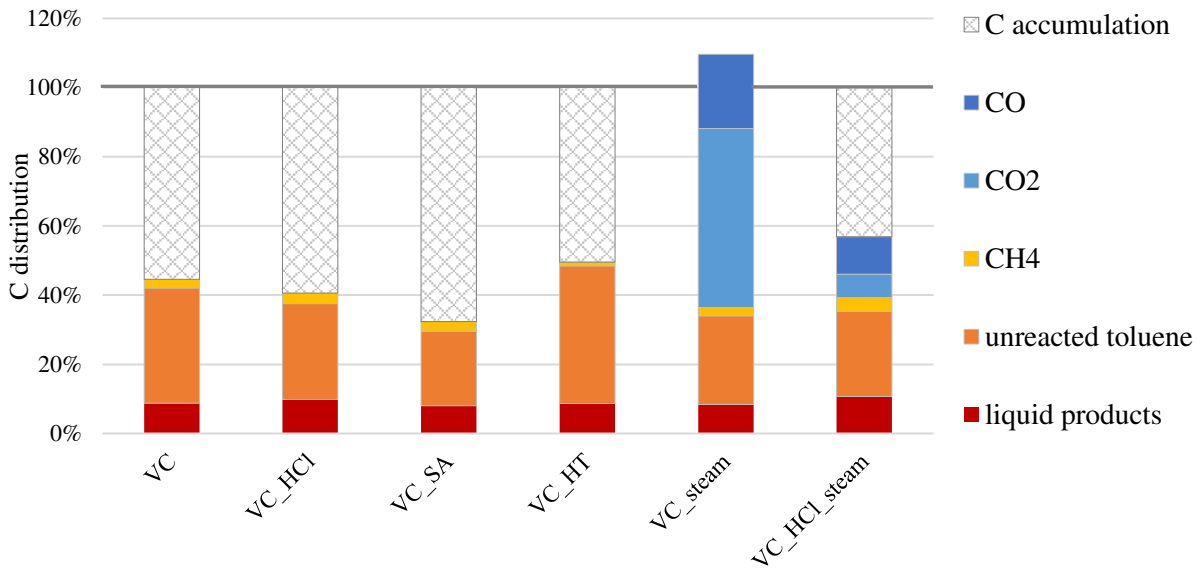

Fig. 13. Carbon distribution in the reaction products based on the amount of C fed with the toluene during conversion under inert (N_2) and oxidising (steam) atmosphere

3.4. The gasification reactivity and catalytic properties of biochar based on AAEM content and surface area

Four char samples (the untreated VC and three modifications) were evaluated as catalysts for toluene decomposition, while the CO_2 gasification reactivities of the fresh and spent materials were determined using TGA. The main physicochemical properties of the chars were analysed to identify the differences between the samples, focusing primarily on their surface area and inherent inorganic content. This approach allowed for comparing the performance of the chars in terms of the parameters generally attributed to high reactivity and good catalytic properties of carbonaceous materials. Interestingly, it was observed that the char reactivity and catalytic efficiency were not equally affected by the applied pre-treatments. This result suggests that different features of the char play crucial roles in determining its gasification reactivity and

782 catalytic properties. Therefore, an attempt was made to understand how the most important
783 parameters of the char (surface area, surface functionalities, and inorganic content) influence
784 the char performance (reactivity, R_{50}, and toluene conversion, η_T).

785 In Fig. 14a, the R_{50} values of the chars are compared with the K content, which is one of the
786 main and most reactive AAEM species. A general trend of increasing gasification reactivity
787 with increasing concentration of K is clear. The most drastic difference in the chars' K content,
788 introduced by acid washing and steam activation, resulted in R_{50} values that were 10 times lower
789 (VC_HCl) and two times higher (VC_SA) than the VC. The char reactivity was most likely
790 influenced by other parameters as well, e.g., a decrease in R_{50} was observed for coke-covered
791 materials. Both the pre-treatment and application for toluene conversion also affected the
792 structural parameters of the chars, including the functional groups, pore size distribution, and
793 likely the organisation of the carbon lattice within the chars, i.e., the presence of the unsaturated
794 carbons. As a result, it is impossible to isolate the effect of the inorganics on the reactivity;
795 however, a relatively good linear fit of the reactivity with respect to the potassium content was
796 observed in this study, as described by Eq. 8,

797 $$R_{50} = 0.00004C_K + 0.058 \quad (8)$$

798 where C_K is the potassium content (ppm) in the char.

799 The plot of the R_{50} values as a function of the BET surface area of the chars, which varied
800 drastically among the analysed samples, revealed no clear correlation (Fig. 14b). Despite the
801 small decrease in the reactivity of each fresh char with the reduction in surface area, resulting
802 from the exposure to toluene, the main differences in the gasification reactivity was observed
803 between the main types of chars with the most diverse AAEM content (i.e., between the VC,
804 VC_HCl, and VC_SA groups), regardless of the significant changes in their surface areas

caused by their interactions with toluene. There was no clear relationship between the reactivity of chars and the development of their surface functional groups observed by ATR-FTIR.

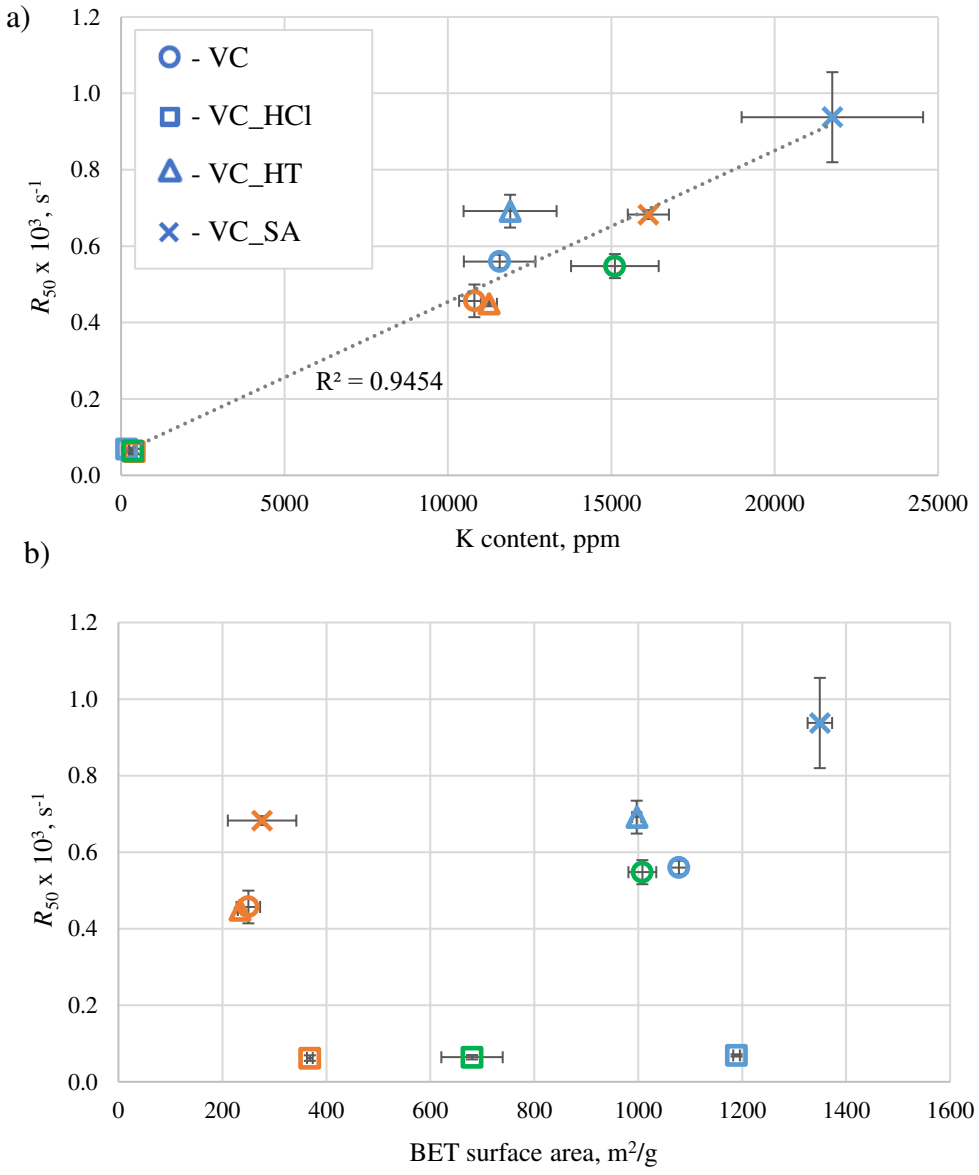

Fig. 14. The reactivity, R_{50}, of the fresh (blue) chars and the recovered chars after 50 min of toluene pyrolysis (orange) and steam reforming (green) plotted against (a) the K content in the char and (b) the BET surface area determined from the N_2 adsorption isotherm

The reactivity of the char was affected substantially by its inherent inorganic content, whereas the wide variations in the surface area did not contribute significantly to the gasification rate of

these materials. In contrast, the catalytic activity of the char towards pyrolytic toluene conversion was largely unaffected by the presence of inherent inorganics. The acid-washed char (VC_HCl) performed better than the untreated sample, despite the removal of AAEM species, while the steam-activated (VC_SA) char contained an increased metal content and an improved catalytic efficiency. These results indicated that there was no clear correlation between the catalyst's inorganic content and its toluene conversion capabilities. However, the changes in the surface area and pore size distribution, which are also commonly attributed to the catalytic properties of the materials, correspond relatively well with the observed differences in toluene pyrolysis, as presented in Fig. 15. The useful surface area employed in this comparison was calculated from the 2D-NLDFT pore size distribution and determined as the cumulative surface area of the pores with sizes larger than the kinetic diameter of toluene (5.85 Å), because only those pores are expected to participate in the toluene conversion. The four fresh chars differed in terms of their inorganic content and O-functional groups, which could be expected to obscure the correlation between the surface area and toluene conversion. However, the linear relationship between η_T (%) and the useful surface area was observed for both toluene feeding times, as described by Eq. 9 and 10,

$$\eta_T(t = 50\text{min}) = 0.069A_u + 23.7 \quad (9)$$

$$\eta_T(t = 30\text{min}) = 0.068A_u + 33.4 \quad (10)$$

where A_u is the useful surface area (m^2/g). The similarity between the slopes of both fitted functions suggests a uniform conversion mechanism that depends mainly on the char's capacity for coke accumulation.

Therefore, it can be expected that under an inert atmosphere, the inherent inorganic content in the char has a negligible effect on the conversion of toluene, and that the catalytic properties are determined mainly by the char's structural parameters. For chars with a similar nature (i.e.,

obtained from the same feedstock and only slightly modified), the useful surface area seemed to be the main feature affecting the toluene conversion. However, further investigations are required to confirm this hypothesis. The results of this study appear to contradict Fuentes-Cano et al.'s observation [25] of decreased naphthalene removal over acid-washed coal char, suggesting that some important process parameters must be accounted for, while examining the role of inorganics in the tar conversion process. Different procedures for samples preparation were applied in the two studies. Steam activation performed after the removal of inorganics may have affected the char activation process (e.g., inhibited the formation of O-functionalities on the surface). Moreover, the lack of the methyl group in naphthalene could have impacted its sensitivity to catalysis promoted by AAEM species. Indeed, our previous work regarding the conversion of benzene suggested that non-methylated aromatics have different sensitivity to the catalyst compared with more reactive, methylated species [36].

However, the most important difference can be traced back to the feedstock used for the char preparation; the metals in coal are present in the form of clusters, contrary to the well-dispersed ions and salts in biomass. Therefore, it is plausible that the inorganics in the coal char examined by Fuentes-Cano et al. [25] remained in the form of agglomerates, as indicated by the inorganic clusters observed in the SEM-EDS scans of the coal char [25], whereas the K and Ca elements were well-dispersed on the biochar surface (Fig. 5e). Since the metal particles and clusters have stronger catalytic effects than the structures integrated in the carbon matrix (e.g., C–O–M phenolates [20,38]), the inherent inorganics in coal and biomass likely have different affinities for catalysing tar conversion reactions.

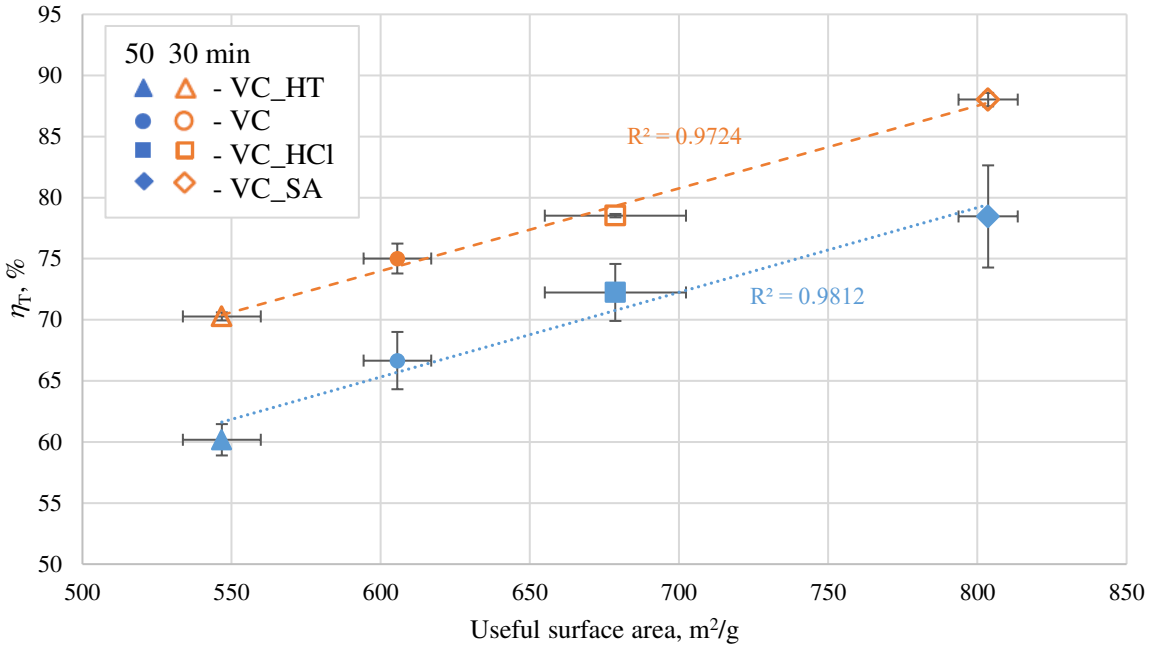

862

863 Fig. 15. Correlation between the pyrolytic toluene conversion (η_T) during the 30- and 50-min
864 tests and the useful surface area (pores >5.85 Å) of the chars

865

866 **4. Conclusions**

867 This work examined the effect of the surface area and inherent inorganic contents of wood-
868 derived char on its gasification reactivity and catalytic performance. The untreated and
869 modified chars were gasified with CO_2, and they were also used as catalysts for toluene
870 conversion. The goals of the modifications were to change the surface area and inorganic
871 content of the untreated char: acid wash removed the inorganics, steam activation increased the
872 surface area and inorganic concentration, and high-temperature annealing decreased the
873 porosity of the char.

874 The results indicated that the reactivity of the char was strongly correlated with the quantity of
875 AAEM species, yet there was no clear effect of the surface area on the char's gasification rate.
876 Conversely, toluene pyrolytic conversion over the char was unaffected by changes in the

concentration of inorganics, yet it correlated well with the surface area available for the reaction with toluene. Therefore, it was concluded that enhanced oxygen adsorption on the char surface due to the AAEM species incorporated in the carbonaceous matrix significantly increased char gasification rate, but it did not contribute to toluene reactions on the surface. The microcrystalline structure of the char is rich in unsaturated carbons that can attract volatile compounds, so the determining factor for the toluene removal efficiency was the area of the char surface that was available for toluene adsorption (i.e., the area comprised of pores with a size greater than the kinetic diameter of toluene). However, the inorganics in the char could indirectly enhance toluene conversion during the reforming process, by catalysing the gasification, and thus activation, of the char.

It is important to note that the observations presented herein were made for one type of catalyst and one tar-representing compound (toluene). Therefore, further research into the catalytic effects of different char properties is required to unambiguously determine their importance. For example, studies regarding conversion of O-containing, polyaromatic, or non-substituted aromatics, and mechanistic investigations of their heterogeneous decomposition will lead to a more comprehensive insight on how different metal species might contribute uniquely to their conversion. Moreover, because the nature of the metal-char bonding is known to have a strong impact on the reactivity of these active sites [20], it is advisable to examine the role of inorganics introduced in a form different to that of the inherent char elements, e.g., using a catalyst impregnated with metal salts.

Acknowledgements

This work was supported by the Statutory Fund of the Faculty of Energy and Environmental Engineering of the Silesian University of Technology.

Appendix A. Supplementary data

Supplementary data to this article can be found online at

References

[1] F. Patuzzi, D. Prando, S. Vakalis, A.M. Rizzo, D. Chiaramonti, W. Tirler, T. Mimmo, A. Gasparella, M. Baratieri, Small-scale biomass gasification CHP systems: Comparative performance assessment and monitoring experiences in South Tyrol (Italy), Energy. 112 (2016) 285–293. https://doi.org/10.1016/j.energy.2016.06.077.

[2] J. Lehmann, S. Joseph, Biochar for environmental management: science, technology and implementation, Routledge, 2015.

[3] E.F. Zama, B.J. Reid, H.P.H. Arp, G.X. Sun, H.Y. Yuan, Y.G. Zhu, Advances in research on the use of biochar in soil for remediation: a review, J. Soils Sediments. 18 (2018) 2433–2450. https://doi.org/10.1007/s11368-018-2000-9.

[4] V. Augustyn, P. Simon, B. Dunn, Pseudocapacitive oxide materials for high-rate electrochemical energy storage, Energy Environ. Sci. 7 (2014) 1597–1614. https://doi.org/10.1039/c3ee44164d.

[5] J. Lee, K.H. Kim, E.E. Kwon, Biochar as a Catalyst, Renew. Sustain. Energy Rev. 77 (2017) 70–79. https://doi.org/10.1016/j.rser.2017.04.002.

[6] F. Nestler, L. Burhenne, M.J. Amtenbrink, T. Aicher, Catalytic decomposition of biomass tars: The impact of wood char surface characteristics on the catalytic performance for naphthalene removal, Fuel Process. Technol. 145 (2016) 31–41. https://doi.org/10.1016/j.fuproc.2016.01.020.

[7] D. Fuentes-Cano, A. Gómez-Barea, S. Nilsson, P. Ollero, Decomposition kinetics of model tar compounds over chars with different internal structure to model hot tar removal in biomass gasification, Chem. Eng. J. 228 (2013) 1223–1233. https://doi.org/10.1016/j.cej.2013.03.130.

[8] G. Ravenni, Z. Sárossy, J. Ahrenfeldt, U.B. Henriksen, Activity of chars and activated carbons for removal and decomposition of tar model compounds – A review, Renew. Sustain. Energy Rev. 94 (2018) 1044–1056. https://doi.org/10.1016/J.RSER.2018.07.001.

[9] S. Hosokai, K. Kumabe, M. Ohshita, K. Norinaga, C.Z. Li, J. Hayashi, Mechanism of decomposition of aromatics over charcoal and necessary condition for maintaining its activity, Fuel. 87 (2008) 2914–2922. https://doi.org/10.1016/j.fuel.2008.04.019.

[10] Y. Shen, Chars as carbonaceous adsorbents/catalysts for tar elimination during biomass pyrolysis or gasification, Renew. Sustain. Energy Rev. 43 (2015) 281–295. https://doi.org/10.1016/J.RSER.2014.11.061.

[11] D. Xu, L. Yang, K. Ding, Y. Zhang, W. Gao, Y. Huang, H. Sun, X. Hu, S.S.A. Syed-Hassan, S. Zhang, H. Zhang, Mini-Review on Char Catalysts for Tar Reforming during Biomass Gasification: The Importance of Char Structure, Energy and Fuels. 34 (2020) 1219–1229. https://doi.org/10.1021/acs.energyfuels.9b03725.

[12] Y. Huang, X. Yin, C. Wu, C. Wang, J. Xie, Z. Zhou, L. Ma, H. Li, Effects of metal catalysts on CO2 gasification reactivity of biomass char, Biotechnol. Adv. 27 (2009) 568–572. https://doi.org/10.1016/j.biotechadv.2009.04.013.

[13] Z. Zhang, S. Pang, T. Levi, Influence of AAEM species in coal and biomass on steam co-gasification of chars of blended coal and biomass, Renew. Energy. 101 (2017) 356–363. https://doi.org/10.1016/J.RENENE.2016.08.070.

947 [14] N.B. Klinghoffer, M.J. Castaldi, A. Nzihou, Influence of char composition and
948 inorganics on catalytic activity of char from biomass gasification, Fuel. 157 (2015) 37–
949 47. https://doi.org/10.1016/j.fuel.2015.04.036.

950 [15] A. Dufour, A. Celzard, V. Fierro, E. Martin, F. Broust, A. Zoulalian, Catalytic
951 decomposition of methane over a wood char concurrently activated by a pyrolysis gas,
952 Appl. Catal. A Gen. 346 (2008) 164–173. https://doi.org/10.1016/j.apcata.2008.05.023.

953 [16] M.H. Kim, E.K. Lee, J.H. Jun, S.J. Kong, G.Y. Han, B.K. Lee, T.-J. Lee, K.J. Yoon,
954 Hydrogen production by catalytic decomposition of methane over activated carbons:
955 kinetic study, Int. J. Hydrogen Energy. 29 (2004) 187–193.
956 https://doi.org/10.1016/S0360-3199(03)00111-3.

957 [17] N. Muradov, F. Smith, A. T-Raissi, Catalytic activity of carbons for methane
958 decomposition reaction, in: Catal. Today, Elsevier, 2005: pp. 225–233.
959 https://doi.org/10.1016/j.cattod.2005.02.018.

960 [18] D. Feng, Y. Zhao, Y. Zhang, S. Sun, S. Meng, Y. Guo, Y. Huang, Effects of K and Ca
961 on reforming of model tar compounds with pyrolysis biochars under H2O or CO2, Chem.
962 Eng. J. 306 (2016) 422–432. https://doi.org/10.1016/J.CEJ.2016.07.065.

963 [19] Y. Wu, J. Wang, S. Wu, S. Huang, J. Gao, Potassium-catalyzed steam gasification of
964 petroleum coke for H2 production: Reactivity, selectivity and gas release, Fuel Process.
965 Technol. 92 (2011) 523–530. https://doi.org/10.1016/j.fuproc.2010.11.007.

966 [20] S.G. Chen, R.T. Yang, The active surface species in alkali-catalyzed carbon gasification:
967 Phenolate (C-O-M) groups vs clusters (particles), J. Catal. 141 (1993) 102–113.
968 https://doi.org/10.1006/jcat.1993.1122.

969 [21] S.G. Chen, R.T. Yang, Mechanism of alkali and alkaline earth catalyzed gasification of

970 graphite by CO2 and H2O studied by electron microscopy, J. Catal. 138 (1992) 12–23.
971 https://doi.org/10.1016/0021-9517(92)90003-Z.

972 [22] H. Zhu, X. Wang, J. Zhang, K. Yao, G. Yu, X. Wang, Investigation of K2CO3-Catalyzed
973 Pyrolysis and Steam Gasification of Coal Char, Energy Technol. 3 (2015) 961–967.
974 https://doi.org/10.1002/ente.201500094.

975 [23] T. Sueyasu, T. Oike, A. Mori, S. Kudo, K. Norinaga, J. Hayashi, Simultaneous Steam
976 Reforming of Tar and Steam Gasification of Char from the Pyrolysis of Potassium-
977 Loaded Woody Biomass, Energy & Fuels. 26 (2012) 199–208.
978 https://doi.org/10.1021/ef201166a.

979 [24] D. Feng, H. Sun, Y. Ma, S. Sun, Y. Zhao, D. Guo, G. Chang, X. Lai, J. Wu, H. Tan,
980 Catalytic Mechanism of K and Ca on the Volatile–Biochar Interaction for Rapid
981 Pyrolysis of Biomass: Experimental and Simulation Studies, Energy & Fuels. (2020)
982 acs.energyfuels.0c01946. https://doi.org/10.1021/acs.energyfuels.0c01946.

983 [25] D. Fuentes-Cano, F. Parrillo, G. Ruoppolo, A. Gómez-Barea, U. Arena, The influence
984 of the char internal structure and composition on heterogeneous conversion of
985 naphthalene, Fuel Process. Technol. 172 (2018) 125–132.
986 https://doi.org/https://doi.org/10.1016/j.fuproc.2017.12.015.

987 [26] C.Z. Li, Importance of volatile-char interactions during the pyrolysis and gasification of
988 low-rank fuels - A review, Fuel. 112 (2013) 609–623.
989 https://doi.org/10.1016/j.fuel.2013.01.031.

990 [27] M. Hervy, S. Berhanu, E. Weiss-Hortala, A. Chesnaud, C. Gérente, A. Villot, D. Pham
991 Minh, A. Thorel, L. Le Coq, A. Nzihou, Multi-scale characterisation of chars mineral
992 species for tar cracking, Fuel. 189 (2017) 88–97.
993 https://doi.org/10.1016/j.fuel.2016.10.089.

994 [28] Z. Bai, H. Chen, W. Li, B. Li, Hydrogen production by methane decomposition over coal
995 char, Int. J. Hydrogen Energy. 31 (2006) 899–905.
996 https://doi.org/10.1016/J.IJHYDENE.2005.08.001.

997 [29] D. Feng, Y. Zhang, Y. Zhao, S. Sun, J. Wu, H. Tan, Mechanism of in-situ dynamic
998 catalysis and selective deactivation of H2O-activated biochar for biomass tar reforming,
999 Fuel. 279 (2020) 118450. https://doi.org/10.1016/j.fuel.2020.118450.

1000 [30] J. Ahrenfeldt, U. Henriksen, T.K. Jensen, B. Gøbel, L. Wiese, A. Kather, H. Egsgaard,
1001 Validation of a continuous combined heat and power (CHP) operation of a two-stage
1002 biomass gasifier, Energy and Fuels. 20 (2006) 2672–2680.
1003 https://doi.org/10.1021/ef0503616.

1004 [31] P. Brandt, E. Larsen, U. Henriksen, High tar reduction in a two-stage gasifier, Energy
1005 and Fuels. 14 (2000) 816–819. https://doi.org/10.1021/ef990182m.

1006 [32] S. Hosokai, J.-I. Hayashi, T. Shimada, Y. Kobayashi, K. Kuramoto, C.-Z. Li, T. Chiba,
1007 Spontaneous Generation of Tar Decomposition Promoter in a Biomass Steam Reformer,
1008 Chem. Eng. Res. Des. 83 (2005) 1093–1102. https://doi.org/10.1205/cherd.04101.

1009 [33] J. Jagiello, J. Kenvin, A. Celzard, V. Fierro, Enhanced resolution of ultra micropore size
1010 determination of biochars and activated carbons by dual gas analysis using N2 and CO2
1011 with 2D-NLDFT adsorption models, Carbon N. Y. 144 (2019) 206–215.
1012 https://doi.org/10.1016/j.carbon.2018.12.028.

1013 [34] P. Ollero, A. Serrera, R. Arjona, S. Alcantarilla, The CO2 gasification kinetics of olive
1014 residue, Biomass and Bioenergy. 24 (2003) 151–161. https://doi.org/10.1016/S0961-
1015 9534(02)00091-0.

1016 [35] A. Korus, A. Samson, A. Szlęk, Catalytic conversion of toluene over a biochar bed under

1017 an inert atmosphere – The comparison of chars from different types of wood and the role
1018 of selected metals, Fuel. 279 (2020) 118468. https://doi.org/10.1016/j.fuel.2020.118468.

1019 [36] A. Korus, A. Szlęk, I. Korus, A. Samson, Catalytic conversion of methylated aromatics
1020 over wood-derived chars – The role of reforming agents and the effect of methyl groups,
1021 Fuel. 280 (2020) 118521. https://doi.org/10.1016/j.fuel.2020.118521.

1022 [37] N.B. Klinghoffer, M.J. Castaldi, A. Nzihou, Catalyst properties and catalytic
1023 performance of char from biomass gasification, Ind. Eng. Chem. Res. 51 (2012) 13113–
1024 13122. https://doi.org/10.1021/ie3014082.

1025 [38] D. Feng, Y. Zhao, Y. Zhang, J. Gao, S. Sun, Changes of biochar physiochemical
1026 structures during tar H2O and CO2 heterogeneous reforming with biochar, Fuel Process.
1027 Technol. 165 (2017) 72–79. https://doi.org/10.1016/j.fuproc.2017.05.011.

1028 [39] D. Fuentes-Cano, L. von Berg, A. Diéguez-Alonso, R. Scharler, A. Gómez-Barea, A.
1029 Anca-Couce, Tar conversion of biomass syngas in a downstream char bed, Fuel Process.
1030 Technol. 199 (2020) 106271. https://doi.org/10.1016/J.FUPROC.2019.106271.

1031 [40] R.M. Silverstein, F.X. Webster, D.J. Kiemle, D.L. Bryce, Spectrometric Identification
1032 of Organic Compounds, 8th ed., Wiley, 2014.

1033 [41] W. Zieliński, A. Rajca, Metody spektroskopowe i ich zastosowanie do identyfikacji
1034 związków organicznych, second ed., Wydawnictwa Naukowo-Techniczne, Warsaw,
1035 2000.

1036 [42] S.C. Manna, S. Mistri, A.D. Jana, A rare supramolecular assembly involving ion pairs
1037 of coordination complexes with a host–guest relationship: synthesis, crystal structure,
1038 photoluminescence and thermal study, CrystEngComm. 14 (2012) 7415–7422.
1039 https://doi.org/10.1039/C2CE25916H.

[43] G.E. Dunn, R.S. McDonald, Infrared spectra of aqueous sodium benzoates and salicylates in the carboxyl-stretching region: chelation in aqueous sodium salicylates, Can. J. Chem. 47 (1969) 4577–4588. https://doi.org/10.1139/v69-758.

[44] N. Montoya Sánchez, A. de Klerk, Oxidative ring-opening of aromatics: Thermochemistry of sodium, potassium and magnesium biphenyl carboxylates, Thermochim. Acta. 645 (2016) 31–42. https://doi.org/10.1016/j.tca.2016.11.002.

[45] Thommes Matthias, K. Katsumi, N.A. V, O.J. P, R.-R. Francisco, R. Jean, S.K.S. W, Physisorption of gases, with special reference to the evaluation of surface area and pore size distribution (IUPAC Technical Report), Pure Appl. Chem. 87 (2015) 1051. https://doi.org/10.1515/pac-2014-1117.

[46] M. Molina-Sabio, M.T. Gonzalez, F. Rodriguez-Reinoso, A. Sepúlveda-Escribano, Effect of steam and carbon dioxide activation in the micropore size distribution of activated carbon, Carbon N. Y. 34 (1996) 505–509. https://doi.org/10.1016/0008-6223(96)00006-1.

[47] M. Hervy, E. Weiss-Hortala, D. Pham Minh, H. Dib, A. Villot, C. Gérente, S. Berhanu, A. Chesnaud, A. Thorel, L. Le Coq, A. Nzihou, Reactivity and deactivation mechanisms of pyrolysis chars from bio-waste during catalytic cracking of tar, Appl. Energy. 237 (2019) 487–499. https://doi.org/10.1016/j.apenergy.2019.01.021.

[48] J. Jae, G.A. Tompsett, A.J. Foster, K.D. Hammond, S.M. Auerbach, R.F. Lobo, G.W. Huber, Investigation into the shape selectivity of zeolite catalysts for biomass conversion, J. Catal. 279 (2011) 257–268. https://doi.org/10.1016/j.jcat.2011.01.019.

[49] C. Fushimi, T. Wada, A. Tsutsumi, Inhibition of steam gasification of biomass char by hydrogen and tar, Biomass and Bioenergy. 35 (2011) 179–185. https://doi.org/10.1016/J.BIOMBIOE.2010.08.017.

[50] P.N. Bhandari, A. Kumar, D.D. Bellmer, R.L. Huhnke, Synthesis and evaluation of biochar-derived catalysts for removal of toluene (model tar) from biomass-generated producer gas, Renew. Energy. 66 (2014) 346–353. https://doi.org/10.1016/J.RENENE.2013.12.017.

[51] Z. Ma, R. Xiao, H. Zhang, Catalytic steam reforming of bio-oil model compounds for hydrogen-rich gas production using bio-char as catalyst, Int. J. Hydrogen Energy. 42 (2017) 3579–3585. https://doi.org/10.1016/j.ijhydene.2016.11.107.

[52] A. Korus, A. Samson, A. Szlęk, A. Katelbach-Woźniak, S. Sładek, Pyrolytic toluene conversion to benzene and coke over activated carbon in a fixed-bed reactor, Fuel. 207 (2017) 283–292. https://doi.org/10.1016/j.fuel.2017.06.088.